Interleukin-33-Activated Islet-Resident Innate Lymphoid Cells Promote Insulin Secretion through Myeloid Cell Retinoic Acid Production

Dalmas, E.; Lehmann, F.M.; Dror, E.; Wueest, S.; Thienel, C.; Borsigova, M.; ... ; Donath, M.Y.

Article

Immunity

Interleukin-33-Activated Islet-Resident Innate Lymphoid Cells Promote Insulin Secretion through Myeloid Cell Retinoic Acid Production

Graphical Abstract

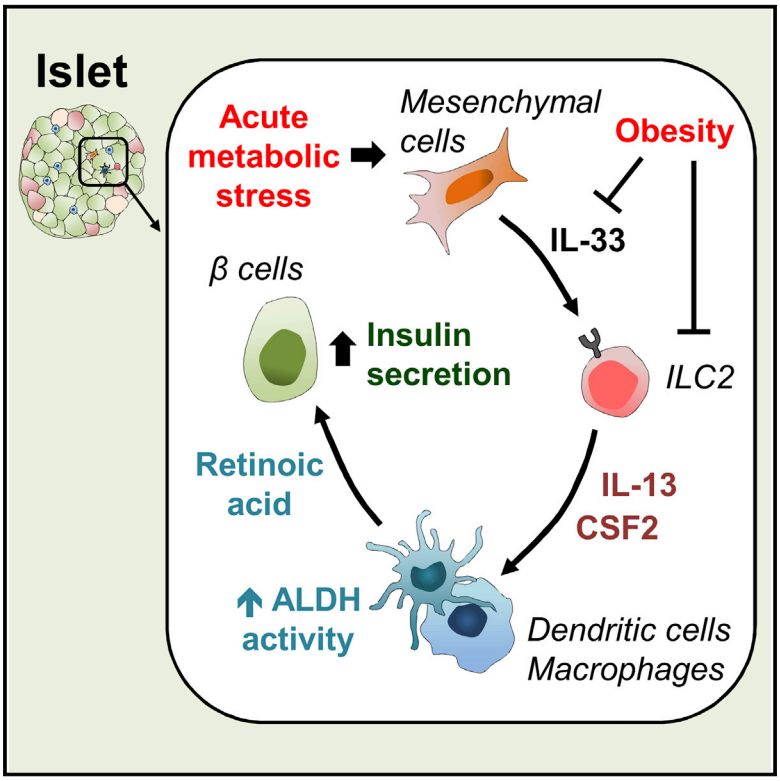

Highlights

- IL-33 is produced by mesenchymal cells in islets
- IL-33 promotes insulin secretion in an ILC2-dependent manner
- ILC2s imprint retinoid acid-producing capacities in myeloid cells in islets

Authors

Elise Dalmas, Frank M. Lehmann, Erez Dror, ..., Marianne Böni-Schnetzler, Daniela Finke, Marc Y. Donath

Correspondence

edalmas@hotmail.fr

In Brief

Pancreatic islet inflammation contributes to the failure of β cell insulin secretion during obesity-associated type 2 diabetes. However, little is known about the role of resident immune cells in this context or in homeostasis. Dalmas and colleagues demonstrate that mesenchymal-cell-derived IL-33 orchestrates an immunometabolic crosstalk in pancreatic islets and that this crosstalk promotes insulin secretion. They show that islet-resident group 2 innate lymphoid cells stimulate retinoic acid production from local myeloid cells and that retinoic acid in turn acts on β cells.

Dalmas et al., 2017, Immunity *47*, 928–942
November 21, 2017
https://doi.org/10.1016/j.immuni.2017.10.015

CellPress

CellPress

Immunity
Article

Interleukin-33-Activated Islet-Resident Innate Lymphoid Cells Promote Insulin Secretion through Myeloid Cell Retinoic Acid Production

Elise Dalmas,[1,2,11,*] Frank M. Lehmann,[2,3] Erez Dror,[1,2] Stephan Wueest,[4] Constanze Thienel,[1,2] Marcela Borsigova,[1,2] Marc Stawiski,[1,2] Emmanuel Traunecker,[2] Fabrizio C. Lucchini,[4] Dianne H. Dapito,[5] Sandra M. Kallert,[2] Bruno Guigas,[6,7] Francois Pattou,[8] Julie Kerr-Conte,[8] Pierre Maechler,[9] Jean-Philippe Girard,[10] Daniel Konrad,[4] Christian Wolfrum,[5] Marianne Böni-Schnetzler,[1,2] Daniela Finke,[2,3] and Marc Y. Donath[1,2]

[1]Clinic of Endocrinology, Diabetes and Metabolism University Hospital Basel, 4031 Basel, Switzerland
[2]Department of Biomedicine, University of Basel, 4031 Basel, Switzerland
[3]University of Basel, Children's Hospital, 4056 Basel, Switzerland
[4]Department of Pediatric Endocrinology and Diabetology and Children's Research Center, University Children's Hospital, Steinwiesstrasse 75, 8032 Zurich, Switzerland
[5]Institute of Food, Nutrition, and Health, ETH-Zürich, Schorenstrasse 16, 8603 Schwerzenbach, Switzerland
[6]Department of Parasitology, Leiden University Medical Center, 2333 ZA Leiden, the Netherlands
[7]Department of Molecular Cell Biology, Leiden University Medical Center, 2333 ZA Leiden, the Netherlands
[8]University Lille, INSERM, CHU Lille, U1190 Translational Research for Diabetes, European Genomic Institute for Diabetes, EGID, 59000 Lille, France
[9]Department of Cell Physiology and Metabolism and Faculty Diabetes Center, Geneva University Medical Centre, Geneva, Switzerland
[10]Institut de Pharmacologie et de Biologie Structurale, Université de Toulouse, CNRS, UPS, 31077 Toulouse, France
[11]Lead Contact
*Correspondence: edalmas@hotmail.fr
https://doi.org/10.1016/j.immuni.2017.10.015

SUMMARY

Pancreatic-islet inflammation contributes to the failure of β cell insulin secretion during obesity and type 2 diabetes. However, little is known about the nature and function of resident immune cells in this context or in homeostasis. Here we show that interleukin (IL)-33 was produced by islet mesenchymal cells and enhanced by a diabetes milieu (glucose, IL-1β, and palmitate). IL-33 promoted β cell function through islet-resident group 2 innate lymphoid cells (ILC2s) that elicited retinoic acid (RA)-producing capacities in macrophages and dendritic cells via the secretion of IL-13 and colony-stimulating factor 2. In turn, local RA signaled to the β cells to increase insulin secretion. This IL-33-ILC2 axis was activated after acute β cell stress but was defective during chronic obesity. Accordingly, IL-33 injections rescued islet function in obese mice. Our findings provide evidence that an immunometabolic crosstalk between islet-derived IL-33, ILC2s, and myeloid cells fosters insulin secretion.

INTRODUCTION

Type 2 diabetes occurs when, as a result of obesity and genetic predisposition, pancreatic-islet insulin secretion fails to compensate for the impaired cell response to insulin (i.e., insulin resistance). It is now recognized that the immune system plays an important role in these processes. Indeed, white adipose tissue (WAT) is a site of inflammation characterized by ongoing activation of type 1 immunity during obesity-associated metabolic dysfunction (Donath et al., 2013). Recent studies suggest a role for resident type 2 immune cells in regulating WAT function and limiting weight gain. Indeed, alternatively activated macrophages, regulatory T cells (Tregs), eosinophils, and group 2 innate lymphoid cells (ILC2s) reside in lean WAT and are altered during obesity (Odegaard and Chawla, 2015). This switch from type 2 to type 1 immunity is supported by findings from studies of two commonly used mouse strains, C57BL/6 and BALB/c, that differ in their immune cell repertoires (for example, see Mills et al., 2000). The T helper 1 (Th1)-cell-permissive C57BL/6 mice are prone to obesity and insulin resistance, whereas the Th2-cell-permissive BALB/c mice are protected against metabolic complications (Montgomery et al., 2013).

During obesity and diabetes, pancreatic islets also undergo inflammation. Glucose, saturated fatty acids, and bacterial products stimulate islet-derived chemokines and cytokines, such as interleukin (IL)-1β, that can then recruit and activate macrophages (Böni-Schnetzler et al., 2009; Calderon et al., 2015; Eguchi et al., 2012; Ehses et al., 2007; Jourdan et al., 2013; Maedler et al., 2002; Nackiewicz et al., 2014; Richardson et al., 2009). Accordingly, anti-inflammatory drugs are in development for the treatment of type 2 diabetes (Donath, 2014). However, islet components of the immune system might also have a beneficial role. Indeed, in experimental β cell ablation models, macrophages promote β cell proliferation and regeneration (Criscimanna et al., 2014; Riley et al., 2015; Xiao et al., 2014). It remains unknown whether other islet-resident immune cells contribute to the maintenance of β cell function.

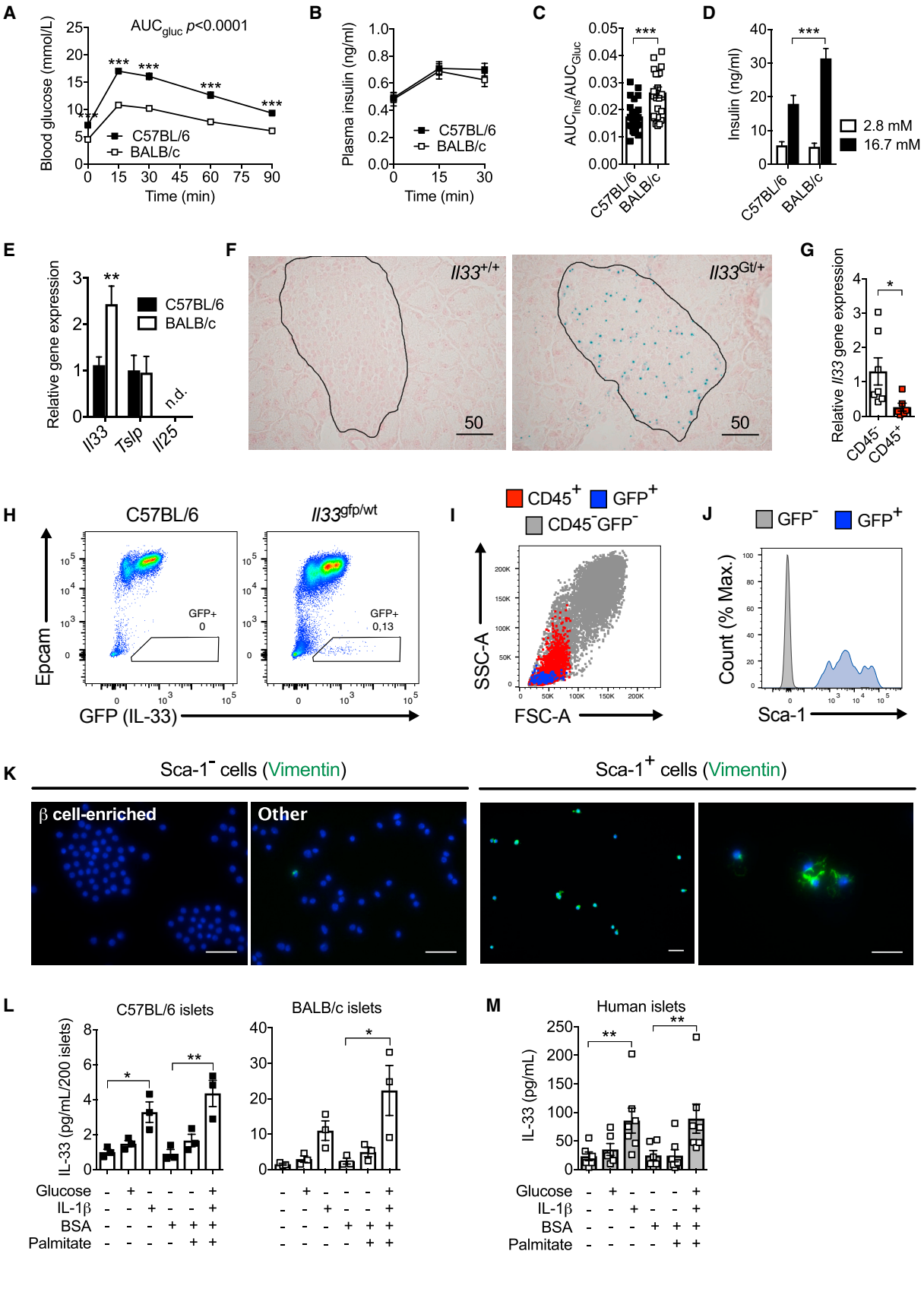

(legend on next page)

In this study, we sought to identify immune cells residing in islets and to investigate their role in physiology and disease. By comparing C57BL/6 and BALB/c mice, we identified mesenchymal-cell-derived IL-33 as an islet immunoregulatory feature. We showed that ILC2s were the primary IL-33-responsive cells in islets and that they elicited the production of retinoic acid (RA) by macrophages and dendritic cells via the secretion of IL-13 and colony stimulating factor 2 (Csf2, also known as GM-CSF). In turn, myeloid-cell-derived RA enhanced β cell insulin secretion. This islet IL-33-ILC2-myeloid-cell circuit was activated after acute β cell injury but altered during obesity.

RESULTS

Islet Mesenchymal Cells Produce IL-33

To extend the role of the Th1-Th2 immune paradigm in metabolic homeostasis to islets, we compared BALB/c and C57BL/6 mouse strains. BALB/c mice displayed a more rapid clearance of blood glucose during intra-peritoneal glucose tolerance tests (GTTs), which reveal insulin secretion and receptor activity, than age-matched C57BL/6 mice (Figure 1A) with comparable body and adipose mass (Figure S1A). Circulating insulin concentrations during GTTs were similar between the groups (Figure 1B), despite the fact that BALB/c mice were more insulin sensitive than C57BL/6 mice (Figure S1B). Besides, mice showed similar production of the uncoupling protein 1 (UCP1) in their brown adipose tissue (Figure S1C). These observations point to increased insulin secretion in BALB/c compared to C57BL/6 mice. Indeed, the insulinogenic index (defined as the ratio of the insulin areas to glucose areas under the curve) during GTTs was higher in BALB/c than in C57BL/6 mice (Figure 1C). To confirm a better β cell function, we tested islets *ex vivo*. Glucose-stimulated insulin secretion (GSIS) was higher in BALB/c than in C57BL/6 islets (Figure 1D) that had comparable insulin content (Figure S1D). We hypothesized that this difference could be due to the BALB/c mouse immune background and measured expression of genes encoding type 2 immune initiators in islets (McKenzie et al., 2014). BALB/c islets showed increased expression of *Il33* but not of *Tslp* (thymic stromal lymphopoietin) and *Il25* compared to C57BL/6 islets (Figure 1E), implying a potential regulatory function for IL-33 in islets.

We next employed an *Il33-LacZ* gene trap ($Il33^{Gt/+}$) reporter strain to visualize endogenous *Il33* expression in the pancreas (Pichery et al., 2012). Galactosidase staining revealed constitutive activity of the *Il33* promoter in islets and, to a much lesser extent, in the exocrine pancreas (located in some vascular beds) of $Il33^{Gt/+}$ mice, and there was no signal in $Il33^{+/+}$ wildtype (WT) mice (Figure 1F and Figure S1E). To study the cellular origin of IL-33, we sorted islet $CD45^+$ immune and $CD45^-$ remaining cells by flow cytometry. *Il33* expression was increased in the $CD45^-$ cells compared to in the immune compartment (Figure 1G). We next analyzed islets isolated from green fluorescent protein (GFP) IL-33 reporter mice by flow cytometry (Kallert et al., 2017; Oboki et al., 2010). GFP production was detected in cells that were $CD45^-FSC^{low}SSC^{low}$ and negative for the Epithelial cell adhesion molecule (Epcam), suggesting a nonepithelial phenotype and thus that the cells were not related to an endocrine origin (Figures 1H and 1I). The IL-33-GFP^+ cells were further classified as positive for the mesodermal stem cell antigen-1 (Sca-1) (Figure 1J), and they preferentially expressed the mesenchymal marker *Vim* (vimentin) and not the smooth-muscle-cell marker *Acta2* (α-SMA) as opposed to β-cell-enriched and other GFP^- subsets (Figure S1F). We confirmed that Sca-1^+ cells (which had been sorted by flow cytometry), rather than β-cell-enriched and other Sca-1^- cells, were the primary population expressing vimentin in islets (Figure 1K).

To characterize IL-33 in islets, we stimulated islets with components of a type 2 diabetes milieu. High concentrations of IL-1β, glucose, and the saturated fatty acid palmitate led to increased amounts of IL-33 mRNA and protein in C57BL/6 and BALB/c mouse islets relative to controls (Figure 1L and Figure S1G), with BALB/c islets overall producing more IL-33 than C57BL/6 islets. Notably, unlike WT controls, IL-33-deficient ($Il33^{-/-}$) mice had undetectable amounts of IL-33 in isolated islet cell lysate (Figure S1H). Similar induction of IL-33 was observed in human islets, especially in response to IL-1β (Figure 1M and Figure S1I). Taken together, our results prompted us to investigate a possible role for mesenchymal-cell-derived IL-33 as an islet stress-signal-regulating endocrine function.

IL-33-Responsive Cells in Islets Are Resident ILC2s

To determine whether IL-33 plays a local role, we sought to identify resident IL-33-responsive cells within islets. In contrast to

Figure 1. *Il33* Expression in Pancreatic Islets

(A and B) (A) Blood glucose and (B) plasma insulin concentrations during GTTs in C57BL/6 and BALB/c mice. n = 25 mice from each of five cohorts.

(C) Insulinogenic index during GTTs. n = 25 mice from each of five cohorts.

(D) Insulin release from islets isolated from C57BL/6 and BALB/c mice during GSIS. n = 13 from each of three independent experiments.

(E) Expression of *Il33*, *Tslp*, and *Il25* in islets isolated from C57BL/6 and BALB/c mice. n = 10 from each of three independent experiments. n.d. = not detectable.

(F) *Il33*-promoter-driven expression of the gene encoding β-galactosidase in pancreata of WT and $Il33^{+/Gt}$ mice. Data are representative of three mice per group. A black line indicates the islet's perimeter. The scale is in μm.

(G) *Il33* expression in islet $CD45^+$ immune and $CD45^-$ cell fractions (sorted by flow cytometry) isolated from C57BL/6 females. n = 6 independent experiments.

(H) GFP and Epcam production in islet cells isolated from $Il33^{gfp/wt}$ and C57BL/6 mice. Data are representative of four independent experiments.

(I) FSC/SSC profiles of islet $CD45^+$, GFP^+, and GFP^- cell fractions. Data are representative of three independent experiments.

(J) Histograms of Sca-1 production by islet GFP^- and GFP^+ cells. Data are representative of four independent experiments.

(K) Vimentin expression in islet Sca-1^- β-cell-enriched cells, other Sca-1^- cells, and Sca-1^+ cells. Data are representative of two independent experiments. Scale bars represent 50 μm.

(L and M) IL-33 protein concentrations in (L) C57BL/6 and BALB/c mouse and (M) human islet cell lysates treated with IL-1β, glucose, bovine serum albumin (BSA), and/or BSA-palmitate. n = 3 (L) independent experiments and 5 (M) donors.

Data are represented as the means ± SEM. *p < 0.05, **p < 0.01, ***p < 0.001; statistical significance (p) was determined by one-way (L and M when normalized to baseline) or two-way analysis of variance (ANOVA) (A, B, D, and E) with Bonferroni's post-hoc test and Student's t test (C and G). See also Figure S1.

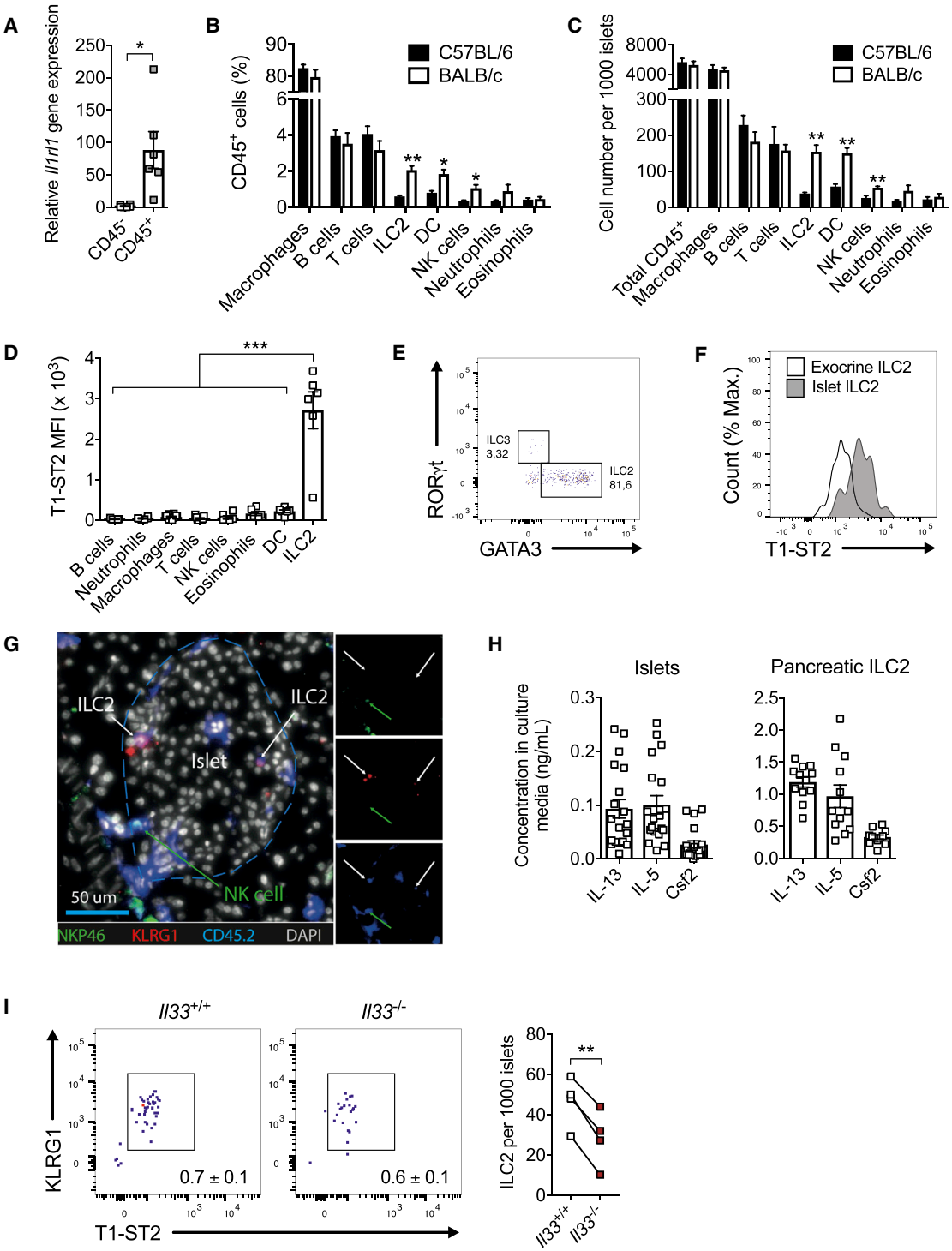

Figure 2. Islet IL-33-Responding Cells Are Resident Group 2 Innate Lymphoid Cells

(A) *Il1rl1* expression in islet CD45$^+$ immune and CD45$^-$ cell fractions (sorted by flow cytometry) isolated from C57BL/6 females. n = 6 independent experiments.

(B and C) Immune-cell profiling of islets isolated from C57BL/6 and BALB/c mice. Cell abundance is expressed as (B) percentage of total CD45$^+$ cells and (C) absolute cell number per 1,000 islets. n = 3–5 independent experiments each (see complete gating strategy in Figure S2A).

(D) Mean fluorescence intensity (MFI) of T1-ST2 produced on islet immune cells. n = 6–12 independent experiments.

(E) Plot of GATA3$^+$ILC2 and RORγt$^+$ILC3 among CD45$^+$Lin$^-$CD90.2$^+$ cells in BALB/c islets. Data are representative of three independent experiments.

(F) Histograms of T1-ST2 production on ILC2 isolated from islets and exocrine stroma of the same mouse pancreas. Data are representative of four independent experiments.

(legend continued on next page)

Il33, the gene encoding the IL33 receptor IL-1-receptor-like 1 (*Il1rl1*, encoding T1-ST2) was expressed more in CD45$^+$ cells than in non-immune cells (Figure 2A). We quantitatively profiled islet-dwelling immune cells of BALB/c and C57BL/6 mice fed a chow diet (see the gating strategy in Figure S2A). Islets contained an average of six pan-CD45$^+$ immune cells per islet; macrophages were the main immune subset (Figures 2B and 2C). BALB/c islets showed increased frequency and cell numbers of specific branches of innate immunity, including ILC2s, dendritic cells, and NK cells, as compared to islets in C57BL/6 mice (Figures 2B and 2C). Islets of both strains contained similar amounts of T and B cells and scarce neutrophils and eosinophils (Figures 2B and 2C). We identified ILC2s as the primary immune subset producing T1-ST2 on their cell surface within islets (Figure 2D). Rare Tregs were detectable in islets and did not produce T1-ST2 (data not shown). Of note, T1-ST2 was also not detectable on the surface of mouse insulin$^+$ β cells (data not shown). ILC2s were lineage negative and produced the cell-surface markers CD90.2 and KLRG1 and the transcription factor GATA binding protein 3 (GATA3) (Figure 2E and Figure S2A). Islet-resident ILC2s were more frequent among CD45$^+$ cells (Figure S2B) and produced higher amounts of T1-ST2 (Figure 2F) than ILC2s isolated from the exocrine stroma of the same pancreas, supporting islet ILC2 specificity. Immunofluorescence analyses confirmed the presence of ILC2s located inside (Figure 2G) or in the periphery (Figure S2C) of islets in *Rag2*$^{-/-}$ mouse pancreas. *Ex vivo*, freshly isolated islets and pancreatic ILC2s sorted by flow cytometry produced type 2 immune cytokines, including IL-5, IL-13, and Csf2, in response to IL-33 and IL-2 (Figure 2H). ILC3s are also known to produce Csf2 (Mortha et al., 2014). Compared to frequencies of GATA3$^+$ ILC2s, frequencies of RAR-related orphan receptor (ROR)γt$^+$ ILC3s were very low in mouse islets and whole pancreata (Figure 2E and Figure S2D), supporting ILC2s as a major source of Csf2 in islets. We next observed that *Il33*$^{-/-}$ mice exhibited a 42% ± 8% decrease in ILC2 number in islets in comparison to WT controls (Figure 2I). Thus, resident ILC2s are the primary responders to IL-33 in islets, and endogenous IL-33 is required for maintaining the islet ILC2 population.

IL-33 Promotes Insulin Secretion

To examine the effects of IL-33 signaling in islet-resident ILC2s *in vivo*, we administered either a single dose (acute) or three doses (chronic) of either saline or mouse recombinant IL-33 every other day to C57BL/6 mice fed a chow diet. Although body and adipose mass were not altered (Figure 3A), acute and chronic IL-33 treatment decreased fasting blood glucose and enhanced glucose clearance in comparison to saline treatment (controls) (Figure 3B). Circulating insulin concentrations during GTTs tended to be boosted after a single injection of IL-33 and reduced upon chronic IL-33 treatment (Figure 3C). Notably, the insulinogenic index was increased upon both acute and chronic IL-33 treatment compared to control treatment (Figure 3D), pointing to increased insulin secretion and progressively enhanced glucose disposal. Accordingly, islets from IL-33-treated mice dose-dependently showed enhanced GSIS in comparison to controls (Figure 3E). IL-33-treated mouse islets also had a better insulin secretion than controls in response to potassium chloride (KCl), known to trigger a robust secretory response (Figure 3F). Insulin content was not different between the GSIS groups (Figures S3A and S3B). Supporting a role for IL-33 to potentiate β cell function and not mass, IL-33 treatment did not alter β cell area (Figure 3G), islet size distribution, and β cell frequency compared to saline groups in this one-week timeframe (Figures S3C and D). Compared to saline treatment or chronic IL-33 treatment, a single dose of IL-33 (three doses of 0.5 μg administered together, that is 1.5 μg) did not significantly improve glucose tolerance or GSIS, which supports time-dependent improvement of β cell function (Figures S3E and S3F).

We next investigated whether the administration of IL-33 improved the insulin response. IL-33 did not affect insulin sensitivity, as demonstrated by both an insulin-tolerance test (Figure 3H) and hyperinsulinemic-euglycemic clamps (Figure 3I and Figure S3G). Tissue glucose uptake was up-regulated in inguinal (Ing)WAT but not in skeletal muscle, epididymal (Epi) WAT, or brown adipose tissue (Figure 3J). Considering that IngWAT is the most prone to beiging of its white adipocytes and that IL-33 has been shown to regulate thermogenesis (Brestoff et al., 2015; Lee et al., 2015; Odegaard et al., 2016), we investigated adipose UCP1 production in our models. Although chronic IL-33 treatment increased *Ucp1* expression in EpiWAT (Figure S3H), no change in UCP1 was observed in IngWAT of IL-33-treated mice compared to in saline groups (data not shown). Importantly, IL-33 treatment still achieved significant improvement in the glucose clearance in *Ucp1*$^{-/-}$ mice compared to controls (Figure 3K), indicating that recruitment of UCP1$^+$ beige fat was dispensable for the IL-33-induced metabolic effect. We also performed pancreas perfusions to study *in situ* GSIS independently of peripheral glucose consumption. In this experimental setting, chronically IL-33-treated mice tended to have increased insulin secretion (Figure S3I), further supporting IL-33 as an insulin secretagogue.

To investigate endogenous IL-33 role in metabolism, we characterized IL-33-deficient mice. We did not observe any difference in body and adipose tissue mass, glucose tolerance, and insulin sensitivity in *Il33*$^{-/-}$ compared to *Il33*$^{+/+}$ littermates when fed a chow diet (Figures S3J–S3L). However, islets from *Il33*$^{-/-}$ chow diet mice displayed an impaired insulin secretion without change in insulin content (Figure S3M) compared to WT islets during *ex vivo* GSIS (Figure 3L). Only when challenged with a high-fat diet did *Il33*$^{-/-}$ mice exhibit obesity and glucose intolerance in comparison to WT controls (Figures S3N and

(G) Picture of C57BL/6 *Rag2*$^{-/-}$ mouse pancreas stained for CD45.2 (blue), KLRG1 (red), NKp46 (green), and DAPI (white). A blue dashed line indicates the islet's perimeter. Data are representative of four mice.

(H) Cytokine concentrations in culture supernatants of BALB/c islets (n = 19 each from six independent experiments) or C57BL/6 pancreatic ILC2s sorted by flow cytometry (n = 12 from each of three independent experiments) in response to IL-33 and IL-2 *ex vivo*.

(I) Representative plots and quantification of ILC2s in islets isolated from *Il33*$^{+/+}$ and *Il33*$^{-/-}$ mice from four independent cohorts.

Data are represented as the means ± SEM. *p < 0.05, **p < 0.01, ***p < 0.001; statistical significance (p) was determined by one-way ANOVA (D) with Bonferroni's post-hoc test and Student's t test (A–C and I when normalized to baseline).

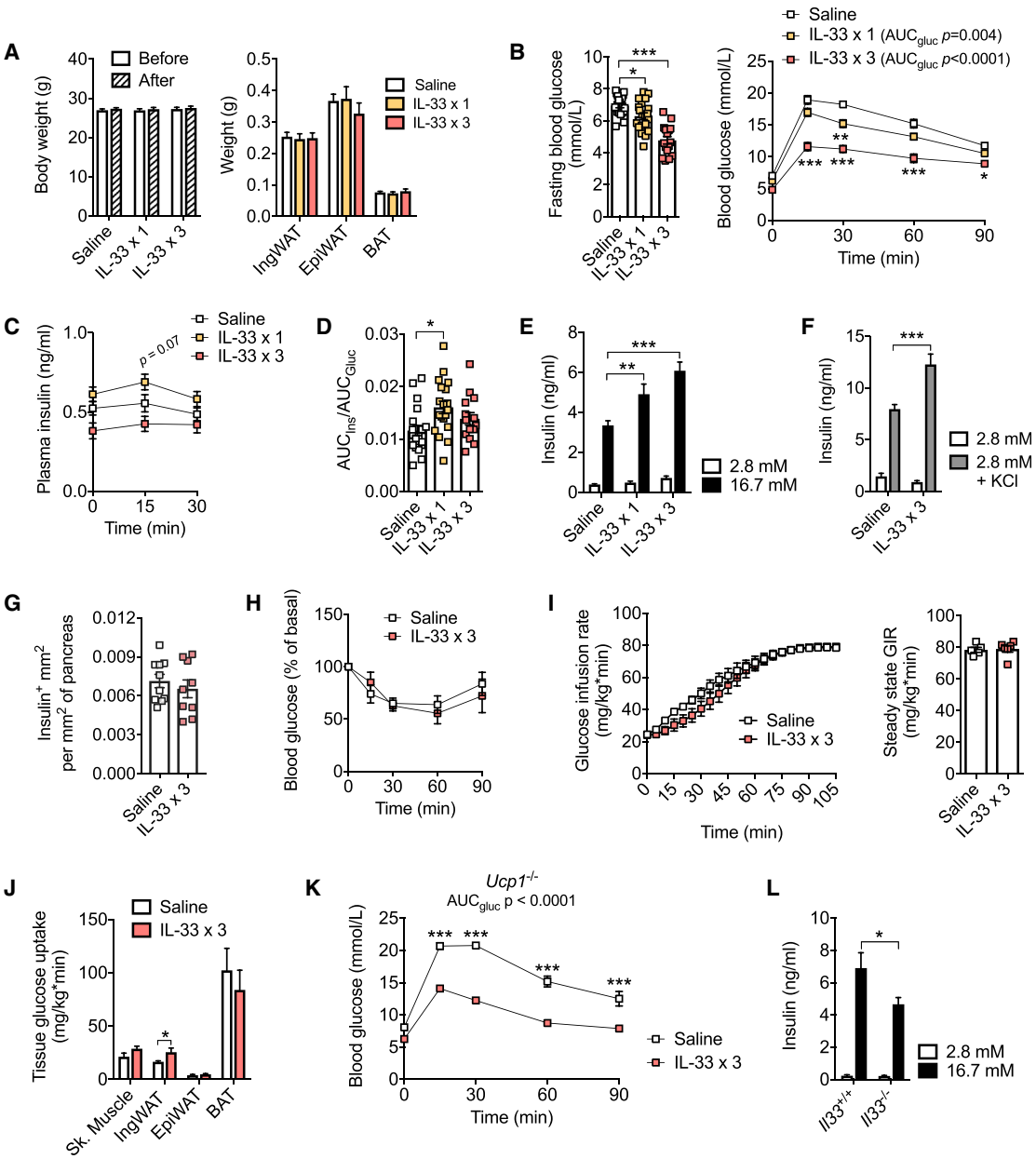

Figure 3. IL-33 Treatment Promotes Glucose Disposal and Insulin Secretion

C57BL/6 mice were treated with one or three doses of saline or IL-33 every other day.

(A–E) (A) Body weight (before and after treatment), IngWAT, EpiWAT, and brown adipose tissue (BAT) mass, (B) fasting glycemia and blood glucose, (C) plasma insulin concentrations, and (D) insulinogenic index during GTTs in saline- and IL-33-treated mice. n = 20, 19, and 15 (except for BAT n = 6 or 7), respectively, from five cohorts. p represents a comparison to the saline group.

(E and F) Insulin release from islets isolated from saline- and IL-33-treated mice during (E) GSIS (n = 19 from each of four independent experiments) and (F) KCl-induced insulin secretion assays (n = 12 from each of three independent experiments).

(G) Quantification of insulin^{+} β cell area in pancreata of saline- and IL-33-treated mice. n = 9 or 10 mice from three cohorts.

(H) Blood glucose concentrations normalized to baseline during insulin tolerance test in saline- and IL-33-treated mice. n = 8 mice each from two cohorts.

(I and J) (I) Glucose infusion rate (GIR) and (J) tissue glucose uptake in skeletal (Sk.) muscle, IngWAT, EpiWAT, and BAT during hyperinsulinemic-euglycemic clamps in saline- and IL-33-treated mice. n = 5 or 6 from each of two cohorts.

(K) Blood glucose concentrations during GTTs in saline- and IL-33-treated *Ucp1*$^{-/-}$ mice. n = 6 or 7 mice representative of two cohorts.

(L) Insulin release from islets isolated from *Il33*$^{+/+}$ and *Il33*$^{-/-}$ littermate mice during GSIS. n = 11 from each of three cohorts.

Data are represented as the means ± SEM. *p < 0.05, **p < 0.01, ***p < 0.001; statistical significance (p) was determined by one-way (B and D) or two-way (B, C, E, F, K, and L) ANOVA with Bonferroni's post-hoc test and Student's t test (J). See also Figure S3.

S3O). Thus, IL-33 could be a critical regulator of β cell function and mediate rapid glucose-lowering effects by stimulation of insulin secretion.

IL-33-Activated ILC2s Promote Insulin Secretion

IL-33 administration increased the number of $CD45^+$ cells and more specifically of ILC2s, dendritic cells and eosinophils in islets compared to controls (Figure 4A and Figures S4A and S4B). Although the number and frequency of macrophages were decreased, T and B cell, NK cell, and neutrophil populations were not affected (Figure 4A and Figure S4A). We also observed higher mRNA expression of typical ILC2-secreted factors including *Il5* (known to mediate eosinophil activation), *Il13*, and *Csf2* in islets from IL-33-treated mice compared to islets in controls (Figure 4B). Down-regulation or no change was observed for expression of other type 2 immune genes including *Areg* (encoding amphiregulin) and type 1 cytokines (Figure S4C).

We next investigated whether IL-33-induced insulin secretion was due to the presence of ILC2s. Three doses of IL-33 or saline were administered to BALB/c WT, *Rag2*$^{-/-}$, and ILC2-deficient *Rag2*$^{-/-}$*Il2rg*$^{-/-}$ mice. We observed that IL-33 significantly improved glucose tolerance and *ex vivo* GSIS in WT and *Rag2*$^{-/-}$ mice but not in *Rag2*$^{-/-}$*Il2rg*$^{-/-}$ mice compared to saline mice (Figures 4C and 4D), with a slight increase in insulin content in WT and *Rag2*$^{-/-}$ mice (Figure S4D). We next treated *Rag2*$^{-/-}$ mice with an anti-CD90.2 antibody, which reduces the number of ILC2s (Monticelli et al., 2011). Anti-CD90.2-treated mouse islets showed a 58 ± 6% decrease in the number of ILC2s (Figure 4E) and tended to have impaired GSIS compared to Immunoglobulin G (IgG) controls (Figure 4F), with no change in insulin content (Figure S4E).

To further confirm that IL-33 promotes insulin production in an ILC2-dependent manner, *Rag2*$^{-/-}$ *Il2rg*$^{-/-}$ mice were adoptively transferred with pancreatic ILC2s and treated with IL-33. ILC2-reconstituted *Rag2*$^{-/-}$*Il2rg*$^{-/-}$ mice supported IL-33-induced ILC2 expansion in their pancreata relative to controls (Figure S4F), without alteration of body and fat mass (Figure S4G). ILC2 transfer was sufficient to rescue IL-33-induced improvement in glucose tolerance test (Figure 4G) and *ex vivo* GSIS (Figure 4H) in *Rag2*$^{-/-}$*Il2rg*$^{-/-}$ mice, with similar circulating insulin concentrations and islet insulin content (Figures S4H and S4I).

We next explored whether ILC2s could act directly on β cells by culturing islets with conditioned media of pancreatic ILC2s. We found that ILC2-conditioned media improved islet GSIS compared to unconditioned medium (Figure 4I), without affecting insulin content (Figure S4J). Collectively, our data indicate that IL-33-induced insulin secretion is not a direct effect of IL-33 on β cells but requires the unique presence of ILC2s and ILC2-secreted factors.

IL-33-ILC2 Axis Elicits RA-Producing Capacities in Islet Myeloid Cells

Islet ILC2s produce IL-13 and Csf2, which are known to imprint RA-producing capacities in macrophages and dendritic cells (Mortha et al., 2014; Yokota et al., 2009). We sought to determine whether our IL-33-ILC2 axis also promoted RA production in islet resident myeloid cells. Vitamin A is oxidized by alcohol dehydrogenases to yield retinal. Retinal is then converted to RA by aldehyde dehydrogenases (ALDH), the major isoform of which is encoded by *Aldh1a2*. IL-33 administration dose-dependently up-regulated *Aldh1a2* expression in islets compared to in saline controls (Figure 5A). We sorted islet macrophages and dendritic cells by flow cytometry from saline- and IL-33-treated mice. Each subset expressed its lineage-characteristic gene, *Emr1* (encoding F4/80) or *Flt3*, respectively, ensuring their identities (Figure S5A). Both islet macrophages and dendritic cells showed up-regulation of *Aldh1a2* mRNA in IL-33-treated mice compared to in controls (Figure 5B). We next measured the relative ALDH activity in islet individual myeloid cells with a fluorescent substrate for ALDH. Islets treated with ALDH inhibitory diethylaminobenzaldehyde were used as a negative control. According to the morphological analysis of islet macrophages, we identified two distinct populations, R1 and R2 (Figure S5B). IL-33 treatment markedly increased ALDH activity in islet R1 macrophages and dendritic cells compared to in controls (Figures 5C and 5D). Although the frequency of granular R2 macrophages was increased in IL-33-treated mice relative to in controls (Figure S5C), R2 macrophage ALDH activity was not inhibited by diethylaminobenzaldehyde, an observation that points toward cell autofluorescence (Figure S5D). Enhanced ALDH activity in both R1 macrophages and dendritic cells was observed in islets isolated from *Rag2*$^{-/-}$ mice but not *Rag2*$^{-/-}$*Il2rg*$^{-/-}$ mice after treatment with IL-33, suggesting that IL-33-induced myeloid RA production is ILC2-dependent (Figures 5E and 5F).

To identify the ILC2-secreted mediators responsible for increased ALDH activity in myeloid cells during IL-33 treatment, we tested the effect of IL-13 and Csf2 *in vitro*. We found that these two molecules together up-regulated the expression of *Aldh1a2* in islet macrophages sorted by flow cytometry (Figure 5G) and in bone marrow-derived dendritic cells (Figure 5H). Of note, recombinant IL-33 did not induce *Aldh1a2* in myeloid cells *in vitro* (data not shown). Islets cultured in the presence of ILC2-conditioned media showed increased *Aldh1a2* expression in comparison to islets cultured in control medium; this increased expression was hampered by the presence of combined anti-IL-13 and anti-Csf2 neutralizing antibodies (Figure 5I). Besides, islets showed increased *Aldh1a2* expression compared to controls when stimulated with IL-33 and IL-2 *in vitro*, suggesting that resident IL-33-responsive ILC2s cells polarize neighboring myeloid cells (Figure 5J). Accordingly, *Il33*$^{-/-}$ mice displayed reduced ALDH activity in islet resident dendritic cells (Figure 5K) but not macrophages (Figure S5E) compared to WT littermates. Collectively, these data support that IL-33-activated ILC2s imprint islet resident myeloid cells with RA-producing capacities in IL-13- and Csf2-dependent ways. Dendritic cells but not macrophages are dependent on endogenous IL-33 to sustain their physiological ALDH activity in islets.

IL-33-Mediated Insulin Secretion Is Dependent on Vitamin A

We next investigated whether IL-33-induced insulin secretion is dependent on RA signaling. The pharmaceutical form of RA, all-*trans* RA, induced insulin secretion in islets *in vitro,* with insulin content similar to that of DMSO controls (Figure 6A and Figure S6A). Many RA biological activities are mediated by RA receptors (RARα, RARβ, and RARγ) or retinoic X receptor (RXRα), whose gene expression can be self-induced (Wu et al., 1992). We observed that all-*trans* RA exclusively up-regulated

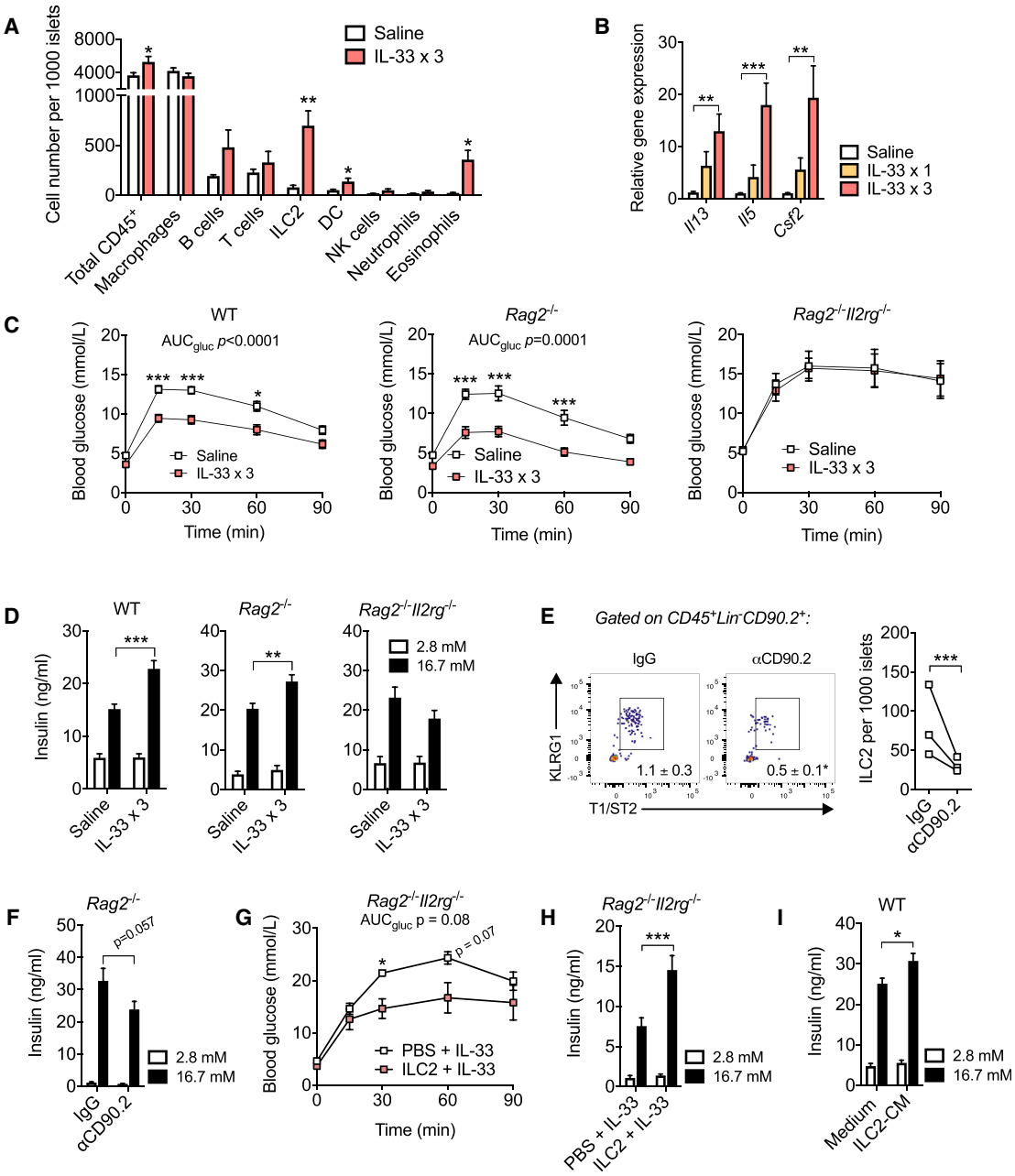

Figure 4. ILC2s Contribute to IL-33-Induced Insulin Secretion

(A) Absolute cell number per 1,000 islets isolated from saline- and IL-33-treated C57BL/6 mice. n = 3–12 independent experiments.

(B) Expression of *Il13*, *Il5*, and *Csf2* in islets isolated from saline- and IL-33-treated mice. n = 10–12 from four cohorts.

(C) Blood glucose concentrations in BALB/c WT, *Rag2*$^{-/-}$ and *Rag2*$^{-/-}$*Il2rg*$^{-/-}$ mice treated with saline or IL-33 during GTTs. n = 10–15 mice from each of three cohorts.

(D) Insulin release during GSIS from islets isolated from saline- and IL-33-treated BALB/c WT (n = 12–13 each), *Rag2*$^{-/-}$ mice (n = 20 each), and *Rag2*$^{-/-}$*Il2rg*$^{-/-}$ mice (n = 14–15 each) from 3 or 4 cohorts.

(E and F) (E) Plot and quantification of ILC2s and (F) insulin release during GSIS (n = 16) from islets isolated from IgG- or anti-CD90.2-treated BALB/c *Rag2*$^{-/-}$ mice. Data are representative of three independent experiments.

(G and H) Pancreatic ILC2 or PBS was transferred to IL-33-treated *Rag2*$^{-/-}$*Il2rg*$^{-/-}$ mice. (G) Blood glucose concentrations during GTTs (n = 3 mice) and (H) insulin release during islet GSIS (n = 16 from four mice) from two cohorts.

(I) Insulin release during GSIS of islets treated with ILC2-conditioned media or control medium. n = 19 per group from four independent experiments.

Data are represented as the means ± SEM. *p < 0.05, **p < 0.01, ***p < 0.001; statistical significance (p) was determined by one-way (B) or two-way (C, D, F, H, and I) ANOVA with Bonferroni's post-hoc test and Student's t test (A, E when normalized to baseline, and G). See also Figure S4.

the expression of *Rarb* (which encodes RARβ) in islets compared to controls (Figure 6B). Accordingly, ILC2-conditioned media failed to increase insulin secretion in islets cultured in the presence of the synthetic RARβ receptor antagonist LE135 in comparison to control islets, and islet insulin content during GSIS was similar in each group (Figure 6C and Figure S6B).

We next conducted a vitamin A deprivation study. To avoid any developmental confounding effects, adult mice were given the diet for 10 weeks. Vitamin A deprivation did not alter body weight nor insulin sensitivity compared to the control chow diet (Figures S6C and S6D). All mice were chronically treated with IL-33 or saline. Notably, vitamin A deficiency did not hinder IL-33-mediated type 2 immunity with similar islet ILC2 and eosinophil numbers between the groups (Figure 6D). In contrast, IL-33 administration failed to induce *Aldh1a2* expression in islets from vitamin-A-deprived mice compared to mice fed the corresponding chow diet and the saline groups (Figure 6E). Reduced ALDH activity was confirmed in islet dendritic cells and to a lesser extent in R1 macrophages from IL-33-treated vitamin A deprived versus chow diet mice (Figure S6E). We did not observe any difference in blood glucose or plasma insulin concentrations during GTTs between the groups (Figure S6F). However, the insulinogenic index was significantly increased in IL-33-treated compared to in saline-treated chow diet mice but not in vitamin-A-deprived mice (Figure 6F), suggesting that IL-33-induced insulin secretion is reduced in the absence of vitamin A. To further investigate the contribution of vitamin A, we performed *ex vivo* experiments with islets. IL-33 treatment increased insulin secretion during both GSIS and KCl-induced insulin secretion in islets from mice fed a control chow diet but not from vitamin-A-deprived mice compared to mice in saline groups (Figures 6G and 6H), without a change in insulin content (Figures S6G and S6H). Therefore, enhancement of β cell function by IL-33 is dependent on dietary vitamin A and its conversion into RA.

Chronic versus Acute Islet Inflammation Regulates the IL-33-ILC2 Axis

To investigate the role of the IL-33-ILC2 axis in a pathological context, mice were fed a chow or high-fat diet. At 3 months, obese mice showed increased body weight and impaired GTTs (Figures S7A and S7B). Notably, obesity was associated with increased plasma insulin concentrations and the absence of glucose-induced insulin production at 15 min compared to baseline (Figure S7C). In comparison to those from controls, islets isolated from obese mice showed a progressive decrease in *Il33* expression and the amount of IL-33 (Figures 7A and 7B). Accordingly, obese mouse islets displayed decreased frequency and number of ILC2s compared to chow diet controls (Figure 7C), together with a late decrease in islet *Aldh1a2* expression (Figure 7D). 7 month-obese mice treated with three doses of IL-33 showed a drastic improvement in glucose clearance during GTTs (Figure 7E), despite no change in body and WAT weights (Figure S7D). IL-33-treated mice overall had lower insulin production than the baseline but showed rescued GSIS at 15 min during GTTs (Figure 7F). Of note, obesity did not hinder IL-33-mediated accumulation of ILC2s or, subsequently, eosinophils in islets of IL-33-treated mice compared to saline controls (Figure S7E).

We next selectively induced β cell injury with a single high dose of streptozotocin (STZ) (Figure S7F). STZ induced a diabetic phenotype characterized by altered glycaemia and insulinaemia compared to buffer-treated mice (data not shown). STZ-treated mice showed increased islet *Il33* expression (Figure 7G) and a more diffuse galactosidase staining than buffer-treated controls (Figure S7G), pointing towards a more active *Il33* promoter. Accordingly, STZ treatment increased the frequency and number of ILC2s in islets compared to in controls (Figure 7H), and increased islet *Aldh1a2* expression (Figure 7I). IL-33 treatment in STZ-induced diabetic mice improved fasting glycemia and prevented further body weight loss compared to in controls (Figure 7J), with a tendency towards increased fasting plasma insulin concentrations on day 9 (Figure S7H) and larger EpiWAT (Figure S7I). In contrast, administration of the ILC2-depleting anti-CD90.2 antibody in STZ-induced diabetic *Rag2*$^{-/-}$ mice tended to worsen fasting glycemia compared to IgG controls (Figure 7K). We did not detect any difference in glycemia when *Il33*$^{-/-}$ and WT littermates were treated with a similar STZ dose (data not shown). Taken together, our results show that the IL-33-ILC2 axis is defective in islets during obesity and is activated following acute β cell stress. ILC2s might not only boost insulin secretion but also contribute to β cell recovery following injury.

DISCUSSION

Our work has established a role for type 2 immunity in the regulation of islet physiology orchestrated by IL-33. Many studies described IL-33 production in mouse tissues at steady state, including in epithelial cells of barrier tissues or endothelial cells in adipose tissue (Liew et al., 2016). In patients suffering from chronic pancreatitis, IL-33 was mainly produced by activated pancreatic stellate cells (Masamune et al., 2010). Here, using two different models of IL-33 reporter mice, we identified IL-33-producing cells as Sca-1^{+}vimentin^{+} mesenchymal cells located inside pancreatic islets. Of note, due to β cell autofluorescence, we cannot exclude the possibility that some IL-33 was produced in β cells in our *Il33*$^{gfp/wt}$ mice. In mouse and human islets, IL-33 production was increased upon stimulation with components of a diabetic milieu, proposing IL-33 as a stress signal in islets. Indeed, designated as an "alarmin," IL-33 is usually released after cell injury to alert the immune system and initiate repair processes (Liew et al., 2016). We detected IL-33 only in islet cell lysate and not in the supernatant. This argues in favor of IL-33 nuclear localization and the requirement for cell death for its proper release. Alternatively, detection of IL-33 in islet cell supernatant might be hindered by its low concentration and rapid inactivation (Liew et al., 2016). Although the role of islet mesenchymal cells remains to be explored, we showed that IL-33 promotes β cell function in chow diet-fed mice. In obese mice, IL-33 injections rescued GSIS during GTTs relative to controls. Conversely, islets from *Il33*$^{-/-}$ mice displayed impaired GSIS compared to WT littermates. Supporting our findings, mice lacking IL-33 receptor T1-ST2 develop hyperglycemia and impaired insulin secretion when fed a high-fat diet (Miller et al., 2010). In contrast to published data linking IL-33 deficiency to obesity, glucose intolerance (Brestoff et al., 2015), and thermogenesis defect (Odegaard et al., 2016), we did not detect any other metabolic alterations in *Il33*$^{-/-}$ mice relative to WT littermates fed a

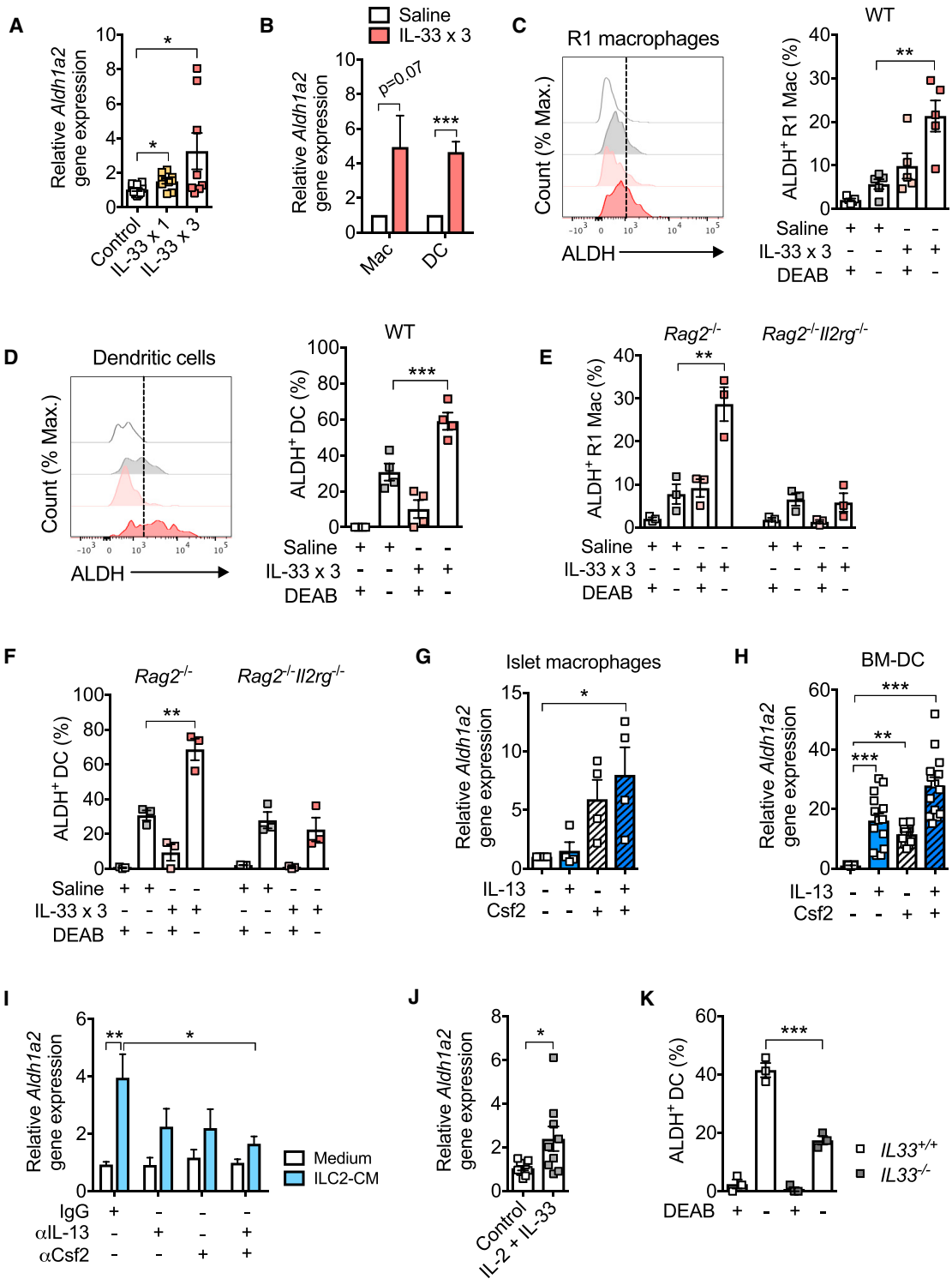

Figure 5. IL-33 Regulates Retinoic-Acid-Producing Capacities in Islet Myeloid Cells

(A) Expression of *Aldh1a2* in islets isolated from saline- and IL-33-treated mice. n = 9 or 10 from three cohorts.

(B) Expression of *Aldh1a2* in islet macrophages (Macs) and dendritic cells (DCs) isolated from saline- and IL-33-treated mice. n = 4 independent experiments.

(C and D) Histograms and frequencies of (C) ALDH$^+$ R1 Macs and (D) ALDH$^+$ DCs in islets isolated from saline- and IL-33-treated C57BL/6 WT mice. n = 5 cohorts. Islets treated with the ALDH inhibitory diethylaminobenzaldehyde (DEAB) were used as a negative control.

(E and F) Frequencies of (E) ALDH$^+$ R1 Macs and (F) ALDH$^+$ DCs in islets isolated from saline- and IL-33-treated BALB/c *Rag2*$^{-/-}$ and *Rag2*$^{-/-}$*Il2rg*$^{-/-}$ mice. n = 3 cohorts.

(legend continued on next page)

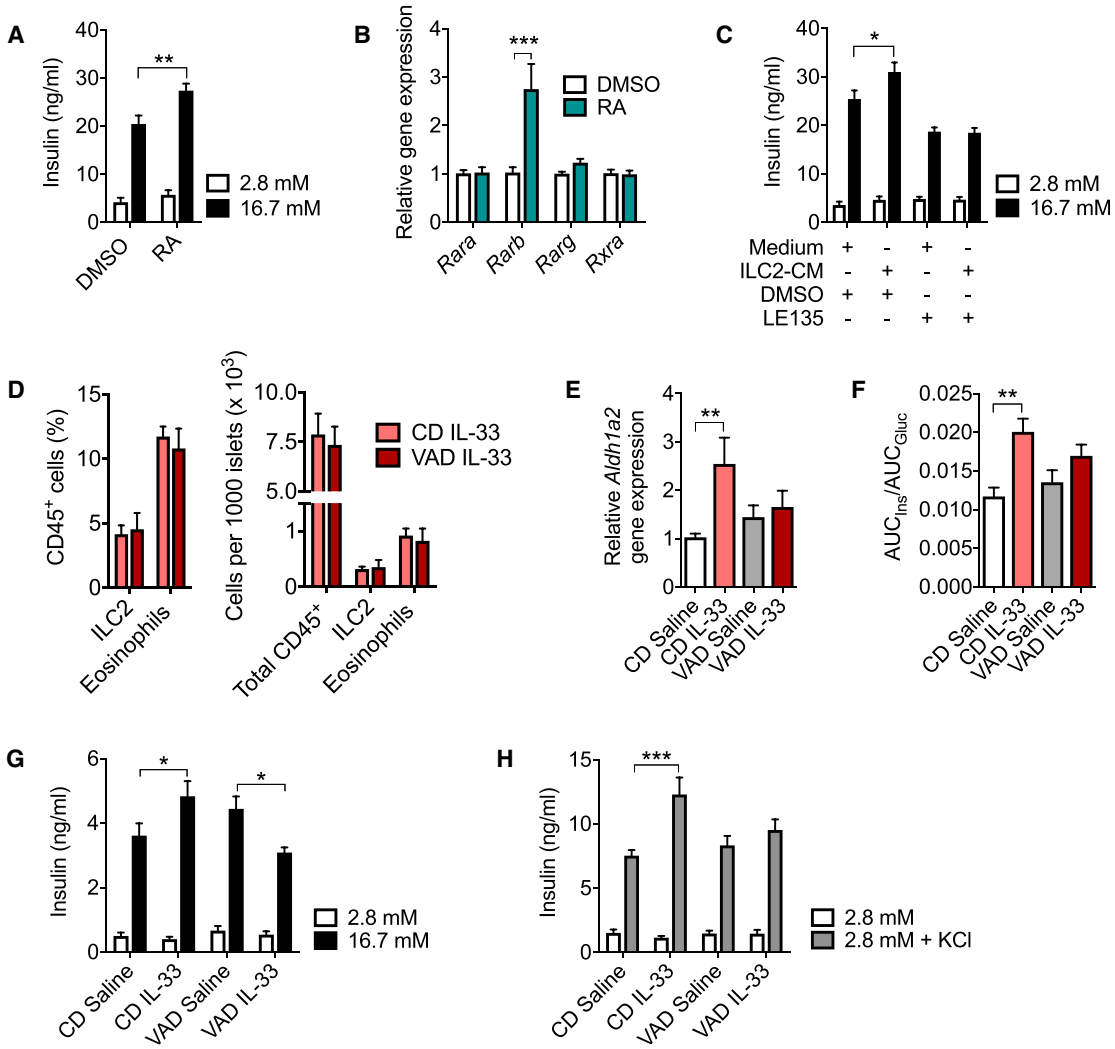

Figure 6. IL-33-Induced Insulin Secretion Requires the Retinoic-Acid Precursor Vitamin A

(A) Insulin release during GSIS from islets treated with DMSO or all-*trans* RA *in vitro*. n = 15 or 16 from each of three independent experiments.

(B) Expression of genes encoding RA receptors in islets treated with DMSO or all-*trans* RA. n = 6 from each of two independent experiments.

(C) Insulin release during GSIS from islets treated *in vitro* with ILC2-conditioned media (CM) or control medium in the presence of DMSO or the retinoic acid receptor (RAR) β antagonist LE135. n = 12 or 13 from each of three independent experiments.

(D–H) C57BL/6 mice fed a control chow diet (CD) or vitamin-A-deficient (VAD) diet were given saline or IL-33 (three doses). (D) Frequencies and absolute numbers of ILC2s and eosinophils in islets (n = 3 from three cohorts), (E) expression of *Aldh1a2* in islets (n = 6–10 from each of four cohorts) and (F) insulinogenic index during GTTs (n = 11–13 mice from each of three cohorts) of saline- and IL-33-treated mice fed a CD or VAD. (G and H) Insulin release during (G) GSIS and (H) KCl-stimulated insulin-secretion assays from islets isolated from saline- and IL-33-treated mice fed a CD or VAD. n = 8 or 9 from each of two cohorts.

Data are represented as the means ± SEM. *p < 0.05, **p < 0.01, ***p < 0.001; statistical significance (p) was determined by one-way ANOVA (E and F) and two-way ANOVA (A–C, G, and H) with Bonferroni's post-hoc test. See also Figure S6.

chow diet. These divergent findings might arise from variations in dietary fat and sucrose content and the use in our study of littermate controls backcrossed on a pure genetic background.

The protective role of IL-33 in obesity has been widely attributed to its modulation of WAT inflammation towards type 2 immunity, which could promote insulin sensitivity (Kolodin et al.,

(G and H) Expression of *Aldh1a2* in (G) islet macrophages (n = 4 independent experiments) or (H) bone-marrow-derived DCs (BM-DCs; n = 10 from three independent experiments) stimulated with IL-13 and Csf2.

(I) Expression of *Aldh1a2* in islets treated *in vitro* with ILC2-conditioned media (CM) or control medium with or without anti(α)-IL-13 and α-Csf2 neutralizing antibodies. n = 8 or 9 per group from three independent experiments.

(J) Expression of *Aldh1a2* in islets isolated from BALB/c mice and stimulated *in vitro* with IL-2 and IL-33. n = 9 per group from three independent experiments.

(K) Frequencies of ALDH$^+$ DCs in islets isolated from *Il33*$^{+/+}$ and *Il33*$^{-/-}$ littermates. n = 3 cohorts.

Data are represented as the means ± SEM. *p < 0.05, **p < 0.01, ***p < 0.001; statistical significance (p) was determined by one-way ANOVA (A and C-H) and two-way ANOVA (I and K) with Bonferroni's post-hoc test and Student's t test (B and J). See also Figure S5.

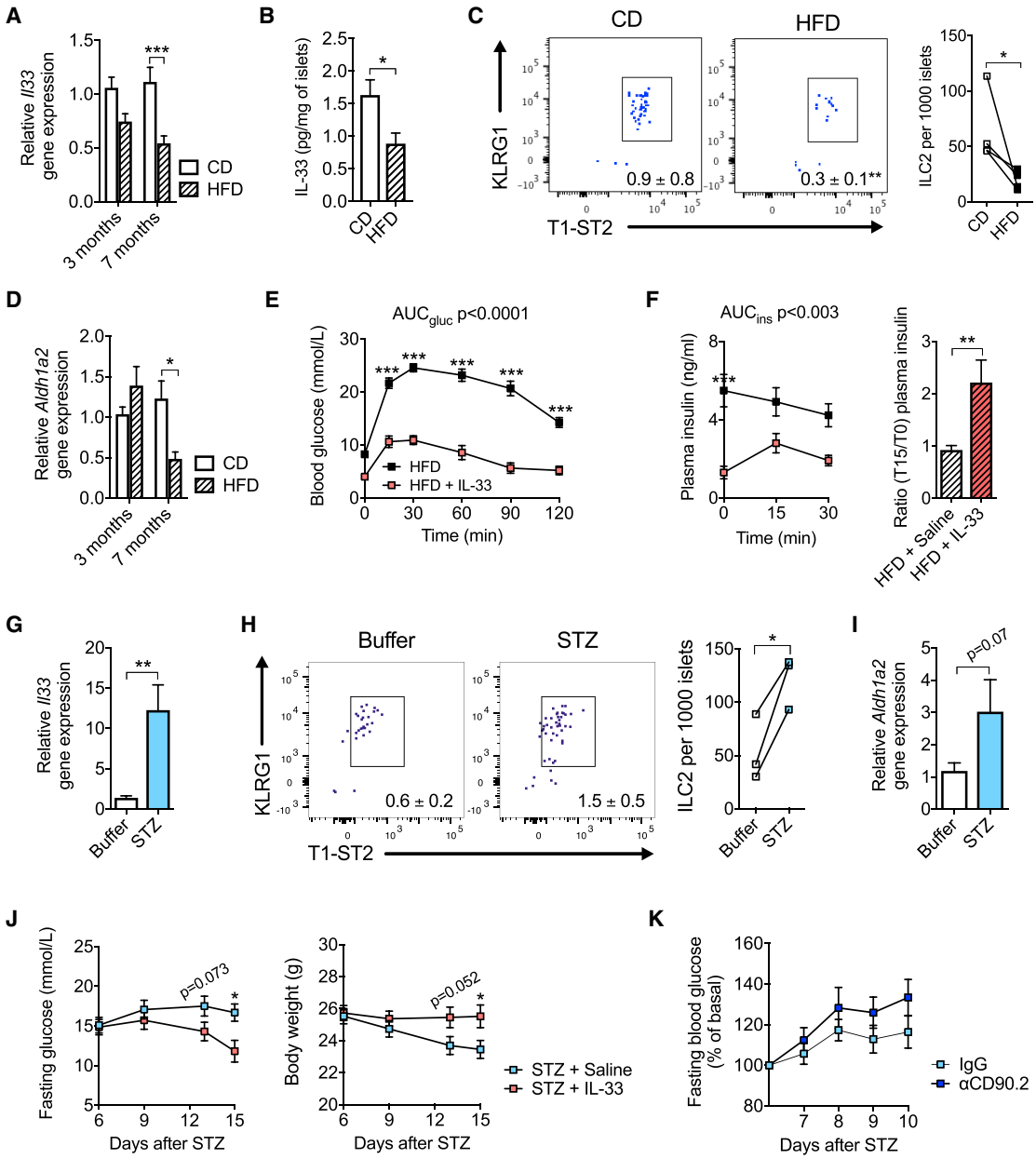

Figure 7. The IL-33-ILC2 Axis Is Altered during Chronic versus Acute Islet Stress

(A) Expression of *Il33* in islets isolated from mice fed a normal chow diet (CD) or a high-fat diet (HFD) for 3 and 7 months. n = 12–17 from each of three cohorts.

(B) IL-33 concentrations in islet cell lysate of mice fed a CD or HFD for 3 months. n = 6-8 each from 2 cohorts.

(C) Plot, frequencies, and absolute numbers of ILC2s in islets isolated from mice fed a CD or a HFD for 3 months. Gated on $CD45^+Lin^-CD90.2^+$ cells. Data are representative of four independent cohorts.

(D) Expression of *Aldh1a2* in islets isolated from mice fed a CD or a HFD for 3 and 7 months. n = 12–17 from each of three cohorts.

(E and F) (E) Blood glucose and (F) plasma insulin concentrations during GTTs in mice fed a HFD for 7 months and treated with saline or IL-33 (three doses). Ratio of insulin secretion between 0 and 15 min is shown. n = 10 mice from each of two cohorts.

(G) Expression of *Il33* in islets isolated from buffer or STZ-treated mice on day 15 after injection. n = 6 or 7 from each of two cohorts.

(H) Plot, frequencies, and absolute numbers of ILC2s in islets isolated from buffer-or STZ-treated mice on day 15 after injection. Cells were gated on $CD45^+Lin^-CD90.2^+$ cells. Data are representative of three independent cohorts.

(I) Expression of *Aldh1a2* in islets isolated from buffer- or STZ-treated CD mice on day 15 after injection. n = 6 or 7 from each of two cohorts.

(J) Mice were treated with STZ on day 0. From day 6, mice were administered saline or IL-33 (three doses) every other day. Fasting blood glucose concentrations and body weight were monitored. n = 12 or 13 mice from three cohorts.

(K) $Rag2^{-/-}$ mice were given STZ on day 0 and treated with IgG or anti(α)-CD90.2 antibody on days 6 and 8. Fasting blood glucose concentrations were monitored and normalized to baseline. n = 9 or 10 mice from three cohorts.

Data are represented as the means ± SEM. *p < 0.05, ***p < 0.001; statistical significance (p) was determined by two-way ANOVA (A and D-F) with Bonferroni's post-hoc test and Student's t test (B, C, and F–J). See also Figure S7.

2015; Miller et al., 2010; Molofsky et al., 2013; Molofsky et al., 2015; Vasanthakumar et al., 2015). In mice with genetic or diet-induced obesity, IL-33 treatment improved glucose homeostasis compared to in controls. However, this phenotype was not associated with enhanced insulin sensitivity (Miller et al., 2010; Vasanthakumar et al., 2015). Here, we also showed that IL-33 treatment in chow diet mice improved glycemia independently of insulin sensitivity. Recently, IL-33 was shown to elicit WAT beiging and regulate the splicing of *Ucp1* mRNA (Brestoff et al., 2015; Lee et al., 2015; Odegaard et al., 2016). Beige cells have the capacity to consume glucose to produce heat (Kajimura et al., 2015). Although glucose uptake was increased in IngWAT of IL-33-treated mice, chronic IL-33 treatment failed to induce UCP1 protein in WAT compared to in controls, suggesting that our experimental settings are not yet sufficient to stimulate the growth of functional beige fat. Indeed, reports of IL-33-mediated beiging have been based on daily IL-33 injections for more than a week (Brestoff et al., 2015; Lee et al., 2015). Treatment of UCP1-deficient mice confirmed that IL-33 metabolic effects do not rely on recruitment of beige adipocytes to clear the blood glucose. Thus, IL-33 treatment in chow diet-fed mice mainly lowers glycemia by rapid stimulation of insulin secretion in β cells, independently of changes in both insulin sensitivity and adipose beiging. The fact that chronic IL-33 treatment tends to lower insulin concentrations during GTTs might be in response to alternative IL-33 glucose-lowering effects, including glucose consumption by an increased number of activated immune cells.

IL-33 signals through the T1-ST2 receptor, which is mainly produced in immune cells. Although IL-33 induces oxidative stress in the MIN6 β cell line (Hasnain et al., 2014), we did not detect T1-ST2 on the surface of mouse primary β cells but rather detected it on resident immune cells. Although an extensive body of literature focuses on autoimmune diabetic mouse models, there are only a limited number of studies addressing the nature of islet immune cells in WT mice at steady state or in the context of type 2 diabetes. Differences in the methods used to isolate islets could affect immune-cell purity, number, and surface markers. Likewise, the number of islets (from one mouse or pools of mice) could greatly influence the outcome because the number of immune cells ranges from two to ten per islet (Calderon et al., 2015; Calderon et al., 2008; Cucak et al., 2014; Ehses et al., 2007). In our study, we used clean, handpicked islets that were isolated from pools of mice. We confirmed that macrophages are the major immune-cell population existing within normal islets. Yet we also noticed ILC2s, dendritic cells, and NK cells that were more abundant in BALB/c mice than in C57BL/6 mice. Therein, ILC2s located inside and at the periphery of islets were the primary IL-33-responsive cells likely to influence β cell function.

ILC2s are rare yet potent resident cells that mediate tissue protection and repair processes (McKenzie et al., 2014). Our work further extends the understanding of their function to include endocrine regulation. IL-33 treatment in *Rag2*$^{-/-}$ mice, *Rag2*$^{-/-}$*Il2rg*$^{-/-}$ mice, and *Rag2*$^{-/-}$*Il2rg*$^{-/-}$ mice adoptively transferred with ILC2s confirmed that IL-33 does not act directly on β cells but is dependent on the presence of ILC2s and ILC2-secreted factors to promote insulin secretion. IL-33 administration led to a massive accumulation of ILC2s and, subsequently, dendritic cells and eosinophils. Thus, we cannot rule out a possible role for eosinophils in IL-33-mediated metabolic benefits. The IL-33-ILC2 axis also contributed to β cell protection in the context of obesity- and STZ-induced β cell stress, supporting a functional role for this axis. Similar to adipose tissue (Molofsky et al., 2013), obesity was associated with a loss of islet ILC2s. This could be explained in part by the phenotypic plasticity that ILC2s exhibit in response to inflammatory cues, including IL-1β (Ohne et al., 2016), that are elevated during type 2 diabetes in islets (Donath et al., 2013).

Islet ILC2s produced IL-13 and Csf2 and thereby induced RA-producing capacities in approximately 30% of resident dendritic cells and 5% of macrophages under physiological conditions. These percentages were markedly increased after IL-33 treatment but diminished (for dendritic cells) in IL-33-deficient mice. Similar crosstalk has been described in the mouse intestine. Microbiota-driven IL-1β production by macrophages promotes the release of Csf2 by ILC3s, and this release in turn regulates RA production in phagocytes and leads to local Treg homeostasis (Mortha et al., 2014). Our study reveals that similar interactions between islet ILC2s and myeloid cells boost insulin secretion, and these interactions are thus not related to classical immune responses.

Vitamin A or RA-related gene deficiencies block the development of fetal pancreatic islets and abrogate the maintenance of β cell mass and function during adulthood (Brun et al., 2015; Chertow et al., 1987; Martín et al., 2005; Matthews et al., 2004; Pérez et al., 2013; Trasino et al., 2016). We identified resident macrophages and especially dendritic cells as endogenous RA producers in islets. We gave a vitamin-A-deficient diet to adult mice to avoid any developmental issues. In contradiction to published data (Trasino et al., 2016), vitamin-A-deprived mice did not show impaired glucose homeostasis *per se.* However, we observed that IL-33 treatment did not promote β cell function in vitamin-A-deprived mice, in contrast to IL-33 treatment in control mice, supporting the view that IL-33-induced insulin secretion requires vitamin A and its conversion to RA.

In conclusion, our study has identified immunometabolic crosstalk within islets and shown that this crosstalk is initiated by IL-33-releasing mesenchymal cells and leads to an insulin secretagogue effect. IL-33 acts on resident ILC2s that elicit RA-producing capacities in myeloid cells to support insulin secretion. This work represents a step toward improving our understanding of islet resident immune cells and showing that ILC2s can influence β cell physiology. In addition to blocking pro-inflammatory type 1 immunity, selective activation of type 2 immunity could offer therapeutic avenues for immunotherapies in patients suffering from diabetes.

STAR★METHODS

Detailed methods are provided in the online version of this paper and include the following:

- KEY RESOURCES TABLE
- CONTACT FOR REAGENT AND RESOURCE SHARING
- EXPERIMENTAL MODEL AND SUBJECT DETAILS
  - Mice
  - Human pancreatic islets

SUPPLEMENTAL INFORMATION

Supplemental Information includes seven figures and can be found with this article online at https://doi.org/10.1016/j.immuni.2017.10.015.

AUTHOR CONTRIBUTIONS

E.Da. and M.Y.D. conceived the project and wrote the manuscript; E.Da. performed and analyzed the experiments; F.M.L. performed ILC2 sorting and staining and BM-DC experiments; E.Dr., C.T., M.Bor., M. S., M.Böni. and B.G. helped with experiments; E.T. performed cell sorting; S.W., F.C.L. and D.K. performed clamp studies; S.M.K. developed *Il33*$^{gfp/wt}$ mice; F.P. and J.K.C. provided human islets; P.M. performed pancreatic perfusions; J.-P.G. provided *Il33*$^{Gt/+}$ mice; D.H.D. and C.W. performed GTTs on *Ucp1*$^{-/-}$ mice; D.F. provided expertise, reagents, and mice; all co-authors helped with the manuscript.

ACKNOWLEDGMENTS

We are grateful to our excellent technicians, Kaethi Dembinski and Stéphanie Häuselmann; Daniel Pinschewer (University of Basel) for providing *Il33*$^{gfp/wt}$ mice; Angela Bosch and Nicole von Burg for helping with experiments; Friederike Schulze, Shuyang Traub, and Katharina Timper for helpful discussions; and the flow-cytometry, microscopy, and animal facilities of the Department of Biomedicine (University of Basel). E.Da. was financially supported by the University of Basel Research Fund for junior researchers and the European Foundation for the Study of Diabetes and Lilly Research Fellowship. The Swiss National Science Foundation provided support to M.Y.D. (166519) and D.F. (172973).

Received: October 6, 2016
Revised: July 24, 2017
Accepted: October 26, 2017
Published: November 21, 2017

REFERENCES

Böni-Schnetzler, M., Boller, S., Debray, S., Bouzakri, K., Meier, D.T., Prazak, R., Kerr-Conte, J., Pattou, F., Ehses, J.A., Schuit, F.C., and Donath, M.Y. (2009). Free fatty acids induce a proinflammatory response in islets via the abundantly expressed interleukin-1 receptor I. Endocrinology *150*, 5218–5229.

Brasel, K., De Smedt, T., Smith, J.L., and Maliszewski, C.R. (2000). Generation of murine dendritic cells from flt3-ligand-supplemented bone marrow cultures. Blood *96*, 3029–3039.

Brestoff, J.R., Kim, B.S., Saenz, S.A., Stine, R.R., Monticelli, L.A., Sonnenberg, G.F., Thome, J.J., Farber, D.L., Lutfy, K., Seale, P., and Artis, D. (2015). Group 2 innate lymphoid cells promote beiging of white adipose tissue and limit obesity. Nature *519*, 242–246.

Brun, P.J., Grijalva, A., Rausch, R., Watson, E., Yuen, J.J., Das, B.C., Shudo, K., Kagechika, H., Leibel, R.L., and Blaner, W.S. (2015). Retinoic acid receptor signaling is required to maintain glucose-stimulated insulin secretion and β-cell mass. FASEB J. *29*, 671–683.

Calderon, B., Suri, A., Miller, M.J., and Unanue, E.R. (2008). Dendritic cells in islets of Langerhans constitutively present beta cell-derived peptides bound to their class II MHC molecules. Proc. Natl. Acad. Sci. USA *105*, 6121–6126.

Calderon, B., Carrero, J.A., Ferris, S.T., Sojka, D.K., Moore, L., Epelman, S., Murphy, K.M., Yokoyama, W.M., Randolph, G.J., and Unanue, E.R. (2015). The pancreas anatomy conditions the origin and properties of resident macrophages. J. Exp. Med. *212*, 1497–1512.

Chertow, B.S., Blaner, W.S., Baranetsky, N.G., Sivitz, W.I., Cordle, M.B., Thompson, D., and Meda, P. (1987). Effects of vitamin A deficiency and repletion on rat insulin secretion in vivo and in vitro from isolated islets. J. Clin. Invest. *79*, 163–169.

Criscimanna, A., Coudriet, G.M., Gittes, G.K., Piganelli, J.D., and Esni, F. (2014). Activated macrophages create lineage-specific microenvironments for pancreatic acinar- and β-cell regeneration in mice. Gastroenterology *147*, 1106–18.e11.

Cucak, H., Grunnet, L.G., and Rosendahl, A. (2014). Accumulation of M1-like macrophages in type 2 diabetic islets is followed by a systemic shift in macrophage polarization. J. Leukoc. Biol. *95*, 149–160.

Donath, M.Y. (2014). Targeting inflammation in the treatment of type 2 diabetes: time to start. Nat. Rev. Drug Discov. *13*, 465–476.

Donath, M.Y., Dalmas, É., Sauter, N.S., and Böni-Schnetzler, M. (2013). Inflammation in obesity and diabetes: islet dysfunction and therapeutic opportunity. Cell Metab. *17*, 860–872.

Eguchi, K., Manabe, I., Oishi-Tanaka, Y., Ohsugi, M., Kono, N., Ogata, F., Yagi, N., Ohto, U., Kimoto, M., Miyake, K., et al. (2012). Saturated fatty acid and TLR signaling link β cell dysfunction and islet inflammation. Cell Metab. *15*, 518–533.

Ehses, J.A., Perren, A., Eppler, E., Ribaux, P., Pospisilik, J.A., Maor-Cahn, R., Gueripel, X., Ellingsgaard, H., Schneider, M.K., Biollaz, G., et al. (2007). Increased number of islet-associated macrophages in type 2 diabetes. Diabetes *56*, 2356–2370.

Hasnain, S.Z., Borg, D.J., Harcourt, B.E., Tong, H., Sheng, Y.H., Ng, C.P., Das, I., Wang, R., Chen, A.C., Loudovaris, T., et al. (2014). Glycemic control in diabetes is restored by therapeutic manipulation of cytokines that regulate beta cell stress. Nat. Med. *20*, 1417–1426.

Jourdan, T., Godlewski, G., Cinar, R., Bertola, A., Szanda, G., Liu, J., Tam, J., Han, T., Mukhopadhyay, B., Skarulis, M.C., et al. (2013). Activation of the Nlrp3 inflammasome in infiltrating macrophages by endocannabinoids mediates beta cell loss in type 2 diabetes. Nat. Med. *19*, 1132–1140.

Kajimura, S., Spiegelman, B.M., and Seale, P. (2015). Brown and Beige Fat: Physiological Roles beyond Heat Generation. Cell Metab. *22*, 546–559.

Kallert, S.M., Darbre, S., Bonilla, W.V., Kreutzfeldt, M., Page, N., Müller, P., Kreuzaler, M., Lu, M., Favre, S., Kreppel, F., et al. (2017). Replicating viral vector platform exploits alarmin signals for potent CD8(+) T cell-mediated tumour immunotherapy. Nat. Commun. *8*, 15327.

Kolodin, D., van Panhuys, N., Li, C., Magnuson, A.M., Cipolletta, D., Miller, C.M., Wagers, A., Germain, R.N., Benoist, C., and Mathis, D. (2015). Antigen- and cytokine-driven accumulation of regulatory T cells in visceral adipose tissue of lean mice. Cell Metab. *21*, 543–557.

Lee, M.W., Odegaard, J.I., Mukundan, L., Qiu, Y., Molofsky, A.B., Nussbaum, J.C., Yun, K., Locksley, R.M., and Chawla, A. (2015). Activated type 2 innate lymphoid cells regulate beige fat biogenesis. Cell *160*, 74–87.

Liew, F.Y., Girard, J.P., and Turnquist, H.R. (2016). Interleukin-33 in health and disease. Nat. Rev. Immunol. *16*, 676–689.

Maechler, P., Gjinovci, A., and Wollheim, C.B. (2002). Implication of glutamate in the kinetics of insulin secretion in rat and mouse perfused pancreas. Diabetes *51* (*Suppl 1*), S99–S102.

Maedler, K., Sergeev, P., Ris, F., Oberholzer, J., Joller-Jemelka, H.I., Spinas, G.A., Kaiser, N., Halban, P.A., and Donath, M.Y. (2002). Glucose-induced beta cell production of IL-1beta contributes to glucotoxicity in human pancreatic islets. J. Clin. Invest. *110*, 851–860.

Martín, M., Gallego-Llamas, J., Ribes, V., Kedinger, M., Niederreither, K., Chambon, P., Dollé, P., and Gradwohl, G. (2005). Dorsal pancreas agenesis in retinoic acid-deficient Raldh2 mutant mice. Dev. Biol. *284*, 399–411.

Masamune, A., Watanabe, T., Kikuta, K., Satoh, K., Kanno, A., and Shimosegawa, T. (2010). Nuclear expression of interleukin-33 in pancreatic stellate cells. Am. J. Physiol. Gastrointest. Liver Physiol. *299*, G821–G832.

Matthews, K.A., Rhoten, W.B., Driscoll, H.K., and Chertow, B.S. (2004). Vitamin A deficiency impairs fetal islet development and causes subsequent glucose intolerance in adult rats. J. Nutr. *134*, 1958–1963.

McKenzie, A.N.J., Spits, H., and Eberl, G. (2014). Innate lymphoid cells in inflammation and immunity. Immunity *41*, 366–374.

Miller, A.M., Asquith, D.L., Hueber, A.J., Anderson, L.A., Holmes, W.M., McKenzie, A.N., Xu, D., Sattar, N., McInnes, I.B., and Liew, F.Y. (2010). Interleukin-33 induces protective effects in adipose tissue inflammation during obesity in mice. Circ. Res. *107*, 650–658.

Mills, C.D., Kincaid, K., Alt, J.M., Heilman, M.J., and Hill, A.M. (2000). M-1/M-2 macrophages and the Th1/Th2 paradigm. J. Immunol. *164*, 6166–6173.

Molofsky, A.B., Nussbaum, J.C., Liang, H.E., Van Dyken, S.J., Cheng, L.E., Mohapatra, A., Chawla, A., and Locksley, R.M. (2013). Innate lymphoid type 2 cells sustain visceral adipose tissue eosinophils and alternatively activated macrophages. J. Exp. Med. *210*, 535–549.

Molofsky, A.B., Van Gool, F., Liang, H.E., Van Dyken, S.J., Nussbaum, J.C., Lee, J., Bluestone, J.A., and Locksley, R.M. (2015). Interleukin-33 and Interferon-γ Counter-Regulate Group 2 Innate Lymphoid Cell Activation during Immune Perturbation. Immunity *43*, 161–174.

Montgomery, M.K., Hallahan, N.L., Brown, S.H., Liu, M., Mitchell, T.W., Cooney, G.J., and Turner, N. (2013). Mouse strain-dependent variation in obesity and glucose homeostasis in response to high-fat feeding. Diabetologia *56*, 1129–1139.

Monticelli, L.A., Sonnenberg, G.F., Abt, M.C., Alenghat, T., Ziegler, C.G., Doering, T.A., Angelosanto, J.M., Laidlaw, B.J., Yang, C.Y., Sathaliyawala, T., et al. (2011). Innate lymphoid cells promote lung-tissue homeostasis after infection with influenza virus. Nat. Immunol. *12*, 1045–1054.

Mortha, A., Chudnovskiy, A., Hashimoto, D., Bogunovic, M., Spencer, S.P., Belkaid, Y., and Merad, M. (2014). Microbiota-dependent crosstalk between macrophages and ILC3 promotes intestinal homeostasis. Science *343*, 1249288.

Nackiewicz, D., Dan, M., He, W., Kim, R., Salmi, A., Rütti, S., Westwell-Roper, C., Cunningham, A., Speck, M., Schuster-Klein, C., et al. (2014). TLR2/6 and TLR4-activated macrophages contribute to islet inflammation and impair beta cell insulin gene expression via IL-1 and IL-6. Diabetologia *57*, 1645–1654.

Oboki, K., Ohno, T., Kajiwara, N., Arae, K., Morita, H., Ishii, A., Nambu, A., Abe, T., Kiyonari, H., Matsumoto, K., et al. (2010). IL-33 is a crucial amplifier of innate rather than acquired immunity. Proc. Natl. Acad. Sci. USA *107*, 18581–18586.

Odegaard, J.I., and Chawla, A. (2015). Type 2 responses at the interface between immunity and fat metabolism. Curr. Opin. Immunol. *36*, 67–72.

Odegaard, J.I., Lee, M.W., Sogawa, Y., Bertholet, A.M., Locksley, R.M., Weinberg, D.E., Kirichok, Y., Deo, R.C., and Chawla, A. (2016). Perinatal Licensing of Thermogenesis by IL-33 and ST2. Cell *166*, 841–854.

Ohne, Y., Silver, J.S., Thompson-Snipes, L., Collet, M.A., Blanck, J.P., Cantarel, B.L., Copenhaver, A.M., Humbles, A.A., and Liu, Y.J. (2016). IL-1 is a critical regulator of group 2 innate lymphoid cell function and plasticity. Nat. Immunol. *17*, 646–655.

Pérez, R.J., Benoit, Y.D., and Gudas, L.J. (2013). Deletion of retinoic acid receptor β (RARβ) impairs pancreatic endocrine differentiation. Exp. Cell Res. *319*, 2196–2204.

Pichery, M., Mirey, E., Mercier, P., Lefrancais, E., Dujardin, A., Ortega, N., and Girard, J.P. (2012). Endogenous IL-33 is highly expressed in mouse epithelial barrier tissues, lymphoid organs, brain, embryos, and inflamed tissues: in situ analysis using a novel Il-33-LacZ gene trap reporter strain. J. Immunol. *188*, 3488–3495.

Richardson, S.J., Willcox, A., Bone, A.J., Foulis, A.K., and Morgan, N.G. (2009). Islet-associated macrophages in type 2 diabetes. Diabetologia *52*, 1686–1688.

Riley, K.G., Pasek, R.C., Maulis, M.F., Dunn, J.C., Bolus, W.R., Kendall, P.L., Hasty, A.H., and Gannon, M. (2015). Macrophages are essential for CTGF-mediated adult β-cell proliferation after injury. Mol. Metab. *4*, 584–591.

Trasino, S.E., Tang, X.H., Jessurun, J., and Gudas, L.J. (2016). Retinoic acid receptor β2 agonists restore glycaemic control in diabetes and reduce steatosis. Diabetes Obes. Metab. *18*, 142–151.

Vasanthakumar, A., Moro, K., Xin, A., Liao, Y., Gloury, R., Kawamoto, S., Fagarasan, S., Mielke, L.A., Afshar-Sterle, S., Masters, S.L., et al. (2015). The transcriptional regulators IRF4, BATF and IL-33 orchestrate development and maintenance of adipose tissue-resident regulatory T cells. Nat. Immunol. *16*, 276–285.

Wu, T.C., Wang, L., and Wan, Y.J. (1992). Retinoic acid regulates gene expression of retinoic acid receptors alpha, beta and gamma in F9 mouse teratocarcinoma cells. Differentiation *51*, 219–224.

Wueest, S., Mueller, R., Blüher, M., Item, F., Chin, A.S., Wiedemann, M.S., Takizawa, H., Kovtonyuk, L., Chervonsky, A.V., Schoenle, E.J., et al. (2014). Fas (CD95) expression in myeloid cells promotes obesity-induced muscle insulin resistance. EMBO Mol. Med. *6*, 43–56.

Xiao, X., Gaffar, I., Guo, P., Wiersch, J., Fischbach, S., Peirish, L., Song, Z., El-Gohary, Y., Prasadan, K., Shiota, C., and Gittes, G.K. (2014). M2 macrophages promote beta-cell proliferation by up-regulation of SMAD7. Proc. Natl. Acad. Sci. USA *111*, E1211–E1220.

Yokota, A., Takeuchi, H., Maeda, N., Ohoka, Y., Kato, C., Song, S.Y., and Iwata, M. (2009). GM-CSF and IL-4 synergistically trigger dendritic cells to acquire retinoic acid-producing capacity. Int. Immunol. *21*, 361–377.

STAR★METHODS

KEY RESOURCES TABLE

REAGENT or RESOURCE	SOURCE	IDENTIFIER
Antibodies		
Anti-CD16/CD32 (clone 93)	Thermo Fisher Scientific	Cat# 14-0161; RRID: AB_467134
Anti-CD45 PECy7 (clone 30-F11)	Thermo Fisher Scientific	Cat# 25-0451; RRID: AB_469625
Anti-CD45 APC (clone 30-F11)	Thermo Fisher Scientific	Cat# 17-0451; RRID: AB_469392
Anti-CD45 BV605 (clone 30-F11)	Thermo Fisher Scientific	Cat# 103140; RRID: AB_2562342
Anti-CD45.2 Alexa647 (clone 104)	Biolegend	Cat# 109817; RRID: AB_492871
Anti-F4/80 PE (clone BM8)	Thermo Fisher Scientific	Cat# 12-4801; RRID: AB_465923
Anti-F4/80 APC-efluor780 (clone BM8)	Thermo Fisher Scientific	Cat# 47-4801; RRID: AB_2637188
Anti-CD11b PE (M1/70),	Thermo Fisher Scientific	Cat# 12-0112; RRID: AB_465546
Anti-CD11c PE (clone N418)	Thermo Fisher Scientific	Cat# 12-0114; RRID: AB_465551
Anti-CD11c PE-Cy7 (clone N418)	Thermo Fisher Scientific	Cat# 25-0114; RRID: AB_469589
Anti-Ly6G PE (clone 1A8 – Ly6g)	Thermo Fisher Scientific	Cat# 12-9668; RRID: AB_2572719
Anti-CD3 FITC (clone 145-2C11)	Thermo Fisher Scientific	Cat# 11-0031; RRID: AB_464883
Anti-CD3 PE (clone 145-2C11)	Thermo Fisher Scientific	Cat# 12-0031; RRID: B_465497
Anti-CD3 APC (clone 145-2C11)	Thermo Fisher Scientific	Cat# 17-0031; RRID: AB_469315
Anti-CD4 PE (clone GK1.5)	Thermo Fisher Scientific	Cat# 12-0041; RRID: AB_465505
Anti-CD8a PE (clone 53-6.7)	Thermo Fisher Scientific	Cat# 12-0081; RRID: AB_465529
Anti-TCR beta PE (H57-597)	Thermo Fisher Scientific	Cat# 12-5961; RRID: AB_466065
Anti-gamma delta TCR PE (eBioGL3)	Thermo Fisher Scientific	Cat# 12-5711; RRID: AB_465933
Anti-CD19 PE (clone eBio1D3)	Thermo Fisher Scientific	Cat# 12-0193; RRID: AB_657659
Anti-CD19 FITC (clone eBio1D3)	Thermo Fisher Scientific	Cat# 11-0193; RRID: AB_657666
Anti-CD45R (B220) PE (clone RA3-6B2)	Thermo Fisher Scientific	Cat# 12-0452; RRID: AB_465671
Anti-CD45R (B220) PerCp-eFluor710 (clone RA3-6B2)	Thermo Fisher Scientific	Cat# 46-0452; RRID: AB_10717954
Anti-CD45R (B220) PECy7 (clone RA3-6B2)	Thermo Fisher Scientific	Cat# 25-0452; RRID: AB_469626
Anti-NKp46 PE (clone 29A1.4)	Thermo Fisher Scientific	Cat# 12-3351; RRID: AB_996682
Anti-NKp46 efluor660 (clone 29A1.4)	Thermo Fisher Scientific	Cat# 50-3351; RRID: AB_10598806
Anti-NKp46 (polyclonal)	R&D systems	Cat# AF2225; RRID: AB_355192
Anti-NK1.1 PE (clone PK136)	Thermo Fisher Scientific	Cat# 12-5941; RRID: AB_466049
Anti-CD49b (Integrin alpha 2) PE (clone DX5)	Thermo Fisher Scientific	Cat# 12-5971; RRID: AB_466072
Anti-Ter-119 PE (clone Ter-119)	Thermo Fisher Scientific	Cat# 12-5921; RRID: AB_466042
Anti-CD90.2 Pacific Blue (clone 53-2.1)	Thermo Fisher Scientific	Cat# 14-0305; RRID: AB_10645335
Anti-CD90.2 FITC (clone 53-2.1)	Thermo Fisher Scientific	Cat# 11-0902; RRID: AB_465153
Anti-CD90.2 APC-Cy7 (clone 53-2.1)	Biolegend	Cat# 105328; RRID: AB_10613293
Anti-KLRG1 PerCp-eFluor710 (clone 2F1)	Thermo Fisher Scientific	Cat# 46-5893; RRID: AB_10671072
Anti-KLRG1 efluor450 (clone 2F1)	Thermo Fisher Scientific	Cat# 48-5893; RRID: AB_10853191
Anti-KLRG1 PE (clone 2F1/KLRG1)	Biolegend	Cat# 138407; RRID: AB_10574005
Anti-T1-ST2 biotin (DJ8)	mdbioproducts	Cat# 101001B; RRID: AB_947551
Anti-T1-ST2 FITC (DJ8)	mdbioproducts	Cat# 101001F; RRID: AB_947549
Anti-CD25 APC (PC61)	Thermo Fisher Scientific	Cat# 17-0251; RRID: AB_469366
Anti-I-A/I-E efluor450 (clone M5/114.15.2)	Thermo Fisher Scientific	Cat# 48-5321; RRID: AB_1272241
Anti-CD103 PerCp-eFluor710 (clone 2E7)	Thermo Fisher Scientific	Cat# 46-1031; RRID: AB_2573703
Anti-SIGLEC-F Alexa647 (clone E50-2440)	BD bioscience	Cat# 562680
Anti-SIGLEC-F BV421 (clone E50-2440)	BD bioscience	Cat# 562681
Anti-Sca1 PE (clone D7)	Thermo Fisher Scientific	Cat# 12-5981; RRID: AB_466085
Anti-GATA3 efluor660 (clone TWAJ)	Thermo Fisher Scientific	Cat# 50-9966; RRID: AB_1210549

(*Continued on next page*)

Continued

REAGENT or RESOURCE	SOURCE	IDENTIFIER
Anti-ROR gamma (t) PerCP-efluor710 (B2D)	Thermo Fisher Scientific	Cat# 46-6981; RRID: AB_10717956
Anti-UCP1 (polyclonal)	Abcam	Cat# ab10983; RRID: AB_2241462
Anti-Vimentin (clone EPR3776)	Abcam	Cat# ab92547; RRID: AB_10562134
Anti-Insulin (polyclonal)	Dako	Cat# A0564; RRID: AB_10013624
Anti-Insulin Alexa647 (C27C9)	Cell Signaling Technology	Cat# 9008; RRID: AB_2126503
Anti-glucagon Biotin (polyclonal)	Abcam	Cat# AB48287; RRID: AB_880211
In vivo Ultra-LEAF Purified Anti-CD90.2 (clone 30-H12)	Biolegend	Cat# 105310; RRID: AB_313181
In vivo LEAF purified IgG2b (clone RTK4530)	Biolegend	Cat# 400637; RRID: AB_2086803
Anti-mouse IL-13 Functional Grade Purified (clone eBio1316H)	Thermo Fisher Scientific	Cat# 16-7135; RRID: AB_763563
Rat IgG1 K Isotype Control Functional Grade Purified (clone eBRG1)	Thermo Fisher Scientific	Cat# 16-4301; RRID: AB_470154
Anti-mouse GM-CSF Functional Grade Purified (cloneMP1-22E9)	Thermo Fisher Scientific	Cat# 16-7331; RRID: AB_469258
Rat IgG2a K Isotype Control Functional Grade Purified (clone eBR2a)	Thermo Fisher Scientific	Cat# 16-4321; RRID: AB_470157
Biological Samples		
Human islets	Islet transplantation center of Lille (France)	European Consortium for Islet Transplantation
Chemicals, Peptides, and Recombinant Proteins		
Recombinant mouse IL-33 (carrier-free)	Biolegend	Cat# 580506
Recombinant mouse IL-2	Thermo Fisher Scientific	Cat# 14-8021
Recombinant mouse GM-CSF	Thermo Fisher Scientific	Cat# 14-8331
Recombinant mouse IL-13 (carrier-free)	Biolegend	Cat# 575906
Recombinant mouse IL-1β	R&D	Cat# 401-ML-025
Recombinant human IL-1β	R&D	Cat# 201-LB-025
Sodium palmitate	Sigma-Aldrich	Cat# P9767
Bovine Serum Albumin (Fatty acid free – Low endotoxin)	Sigma-Aldrich	Cat# A8806
Collagenase type 4	Worthington	Cat# CLS-4
0.5% Trypsin-EDTA (x10)	Thermo Fisher Scientific	Cat# 15400054
Actrapid Penfill Insulin 100 IU/mL	Novo Nordisk	N/A
Streptozotocin	Sigma-Aldrich	Cat# S0130
All-*trans* retinoic acid	Sigma-Aldrich	Cat# R2625
Synthetic RARβ receptor antagonist LE135	Sigma-Aldrich	Cat# SML0809
Critical Commercial Assays		
ALDEFLUOR kit	StemCell Technologies	Cat# 01700
Mouse/rat insulin kit	Meso Scale Discovery	Cat# K152BZC
Mouse GM-CSF Tissue Culture Kit	Meso Scale Discovery	Cat# K152AXB
V-plex mouse IL-5 kit	Meso Scale Discovery	Cat# K152QSD
U-plex mouse IL-33 assay	Meso Scale Discovery	Cat# K152WFK
U-plex human IL-33 assay	Meso Scale Discovery	Cat# K151WFK
Mouse IL-13 Platinum ELISA	eBioscience	Cat# BMS6015
LacZ Tissue staining kit	InvivoGen	Cat# rep-lz-t
Foxp3/Transcription Factor Staining Buffer Set	Thermo Fisher Scientific	Cat# 00-5523-00
PureLink RNA Micro Kit	Thermo Fisher Scientific	Cat# 12183016
Experimental Models: Organisms/Strains		
Mouse: C57BL/6J	Charles River	Stock No: 000664
Mouse: BALB/cJRj	Janvier Labs	N/A
Mouse: *Il33*$^{+/+}$, *Il33*$^{Gt/+}$and *Il33*$^{-/-}$	Pichery et al., 2012	*Il33*$^{Gt(IST10946B6-Tigm)}$

(*Continued on next page*)

Continued

REAGENT or RESOURCE	SOURCE	IDENTIFIER
Mouse: *Il33*$^{gfp/wt}$	Oboki et al., 2010; Kallert et al., 2017	*Il33*^{tm1Snak} - Accession No: CDB0631K (http://www.clst.riken.jp/arg/mutant%20mice%20list.html)
Mouse: *Rag2*$^{-/-}$	Taconic	129S6/SvEvTac-*Rag2*^{tm1Fwa}
Mouse: BALB/c *Rag2*$^{-/-}$*Il2rg*$^{-/-}$	Jackson Laboratory	C;129S4-Rag2$^{tm1.1Flv}$ Il2rg$^{tm1.1Flv}$/J Stock No: 014593
Mouse: *Ucp1*$^{-/-}$	Jackson Laboratory	B6.129-*Ucp1*^{tm1Kz}/J Stock No: 003124
Software and Algorithms		
FlowJo 10.0.8 software	Tree Star	https://www.flowjo.com/solutions/flowjo/downloads
GraphPad Prism 7 software	GraphPad Software, Inc., Carlifornia	https://www.graphpad.com/
Other		
ECM-coated 24-well plates	Novamed	Cat# E-TCMW-24
High fat diet (58% calories from fat)	Research Diets	Cat# D12331
Vitamin A sufficient control diet	Ssniff special diets GmbH	Cat# E15000
Vitamin A deficient diet	Ssniff special diets GmbH	Cat# E15311

CONTACT FOR REAGENT AND RESOURCE SHARING

Further information and requests for resources and reagents should be directed to and will be fulfilled by the Lead Contact, Elise Dalmas (edalmas@hotmail.fr).

EXPERIMENTAL MODEL AND SUBJECT DETAILS

Mice

Male (and where indicated, female) C57BL/6 and BALB/c wildtype mice were either purchased from Charles River and Janvier Labs, respectively, or were bred in-house. C57BL/6 *Rag2*$^{-/-}$ mice were from Taconic and bred in-house. BALB/c *Rag2*$^{-/-}$ mice were a gift from A. Rolink (University of Basel, Switzerland). BALB/c *Rag2*$^{-/-}$*Il2rg*$^{-/-}$ mice (C;129S4-*Rag2*$^{tm1.1Flv}$ *Il2rg*$^{tm1.1Flv}$/J) were purchased from the Jackson Laboratory. *IL33*$^{Gt/+}$ mice (*Il33*$^{Gt(IST10946B6-Tigm)}$) were generated with insertion of a gene trap cassette containing the LacZ (bgeo) reporter into intron 1 of the *Il33* locus as described previously (Pichery et al., 2012). *IL33*$^{Gt/+}$ mice were first back-crossed for 4 generations with C57BL/6J mice to obtain >98% purity using speed congenics. Homozygote *Il33*$^{Gt/Gt}$ mice are deficient for IL-33 and are referred as *Il33*$^{-/-}$ in the text. *Il33*$^{-/-}$, *Il33*$^{Gt/+}$ and *Il33*$^{+/+}$ mice were all littermates. IL33 reporter mice (*Il33*$^{gfp/wt}$) were derived from the *Il33*$^{-/-}$ mice (*Il33*^{tm1Snak}; (Oboki et al., 2010) obtained by the RIKEN Center for Developmental Biology (Accessory Number: CDB0631K; http://www.cdb.riken.jp/arg/mutant%20mice%20list.html) and generated by intercrossing *Il33*$^{-/-}$ mice with the ZP3-Cre germ line deleter strain to remove the neomycin cassette as previously described (Kallert et al., 2017). *Ucp1*$^{-/-}$ mice (B6.129-Ucp1^{tm1Kz}/J) were purchased from the Jackson Laboratory. Unless otherwise indicated, all mice were fed a chow diet (3436, Provimi Kliba) and sacrificed between 8 to 16 weeks of age. For diet-induced obesity experiments, 4-week-old C57BL/6 mice were fed a high fat diet (D12331, Research Diets; containing 58% calories from fat and supplemented with sucrose) for 3 to 7 months. Mice that did not gain weight under high fat diet were excluded before experimentation. For vitamin A deprivation experiments, 6-week-old C57BL/6 mice were fed a vitamin A deficient diet or the corresponding vitamin A sufficient control diet for 10 weeks (E15311 and E15000; Ssniff special diets GmbH). All animal experiments were conducted according to the Swiss Veterinary Law and Institutional Guidelines and were approved by the Swiss Authorities. All animals were housed under specific pathogen-free conditions, in a 22°C temperature-controlled room with a 12h light – 12h dark cycle and had free access to food and water. All metabolic experiments (glucose and insulin tolerance tests, GSIS and clamps) were performed with littermate mice.

Human pancreatic islets

Human islets were isolated from pancreata of cadaver organ donors at the islet transplantation center of Lille (France) in accordance with the local Institutional Ethical Committee and were provided by the research distribution program through the European Consortium for Islet Transplantation, under the supervision of the Juvenile Diabetes Research Foundation (31-2012-783). Islets were cultured in CMRL-1066 medium (GIBCO) containing 5 mmol/l streptomycin, 2 mM glutamax and 10% FCS (Invitrogen) in humid environment containing 5% CO2. In this study, islets were isolated from five different donors (2 women / 3 men) of 54.4 ± 2.4 years old with a body mass index of 29.2 ± 3.8 kg/m^2.

METHOD DETAILS

Mouse pancreatic islets

To isolate mouse islets, pancreata were perfused through the common bile duct with a HBSS collagenase solution (1.4 g/L; collagenase type 4 Worthington) and digested in the same solution in a 37°C water bath for 26-28 min. After shaking for 15 seconds, pancreata were washed three times with HBSS supplemented with 0.5% bovine serum albumin (BSA) and filtrated through 500 μm and 70 μm cell strainers (Corning). Islets were retained on the 70 μm cell strainer while the cell mixture passing through the 70 μm cell strainer represented the exocrine stoma. Islets from the same condition were double handpicked and pooled into a Petri dish with RPMI-1640 (GIBCO) containing 11.1 mM glucose, 100 units/ml penicillin, 100 μg/ml streptomycin, 2 mM Glutamax, 50 μg/ml gentamycin, 10 μg/ml Fungison and 10% FCS (Invitrogen). Islets were used directly for flow cytometry analysis, RNA isolation or cell culture in humid environment containing 5% CO_2.

In vitro islet treatment

For *Il33* gene expression analyses, 80 handpicked mouse or 2 μL of human islet preparation were cultured on extracellular matrix-coated 24-well plates and treated overnight with recombinant mouse or human IL-1β (10 ng/mL; R&D systems), 33.3 mM of glucose, low endotoxin BSA (Sigma-Aldrich) and/or BSA-coated sodium palmitate (0.5mM; Sigma-Aldrich) before lysis for RNA isolation. For IL-33 protein measurement, 200 handpicked mouse islets or 4 μL of human islet preparation were cultured in suspension in a 96-well plate with similar treatments. After 24h culture, islet-free supernatants were stored at -80°C until analysis. For extraction of the whole-protein fraction of islets, samples were homogenized in lysis buffer (20mM Tris pH 7.5; 150mM NaCl; 10% glycerol; 1% Triton X-100; 1% Na_3VO_4; 1% NaF; 0.5% PMSF and 1 mM EDTA) supplemented with a protease inhibitor cocktail (Roche). When indicated, mouse cultured islets were treated with 1 μM of all-*trans* retinoic acid (R2625; Sigma-Aldrich) for 24h, 2 μM of the synthetic RARβ receptor antagonist LE135 (SML0809; Sigma-Aldrich) for 24h or the neutralizing anti-mouse IL-13 (0.05 μg/mL) and anti-mouse GM-CSF (1.25 μg/mL) Functional Grade Purified antibodies and corresponding isotypes for 48h (Thermo Fisher Scientific). 100 BALB/c islets were stimulated *ex vivo* with IL-2 and IL-33 (10 ng/mg; Thermo Fisher Scientific) for 72h.

In vitro glucose- and potassium chloride-stimulated insulin secretion assays

For *ex vivo* insulin secretion stimulation assays, 20 mouse islets were cultured for 24h and then pre-incubated for 30 min in modified Krebs-Ringer bicarbonate buffer (KRB; 115 mM NaCl, 4.7 mM KCl, 2.6 mM $CaCl_2$ $2H_2O$, 1.2 mM KH_2PO_4, 1.2 mM $MgSO_4$ $2H_2O$, 10 mM HEPES, 0.5% bovine serum albumin, pH 7.4) containing 2.8 mM glucose. KRB was then replaced by KRB with 2.8 mM glucose and collected after 1h to determine the basal insulin release. This was followed by 1h incubation in KRB with 16.7 mM glucose (GSIS) or with KRB with 2.8 mM glucose supplemented with 25 mM of potassium chloride to determine the glucose- or potassium chloride-stimulated insulin release. After supernatant collection, islet protein content was extracted with 0.18 N hydrochloride acid in 70% ethanol to measure insulin content (20 islets in 500 μL). For GSIS following an *in vitro* treatment, islets were resting for 48h and then treated for 24h with all-*trans* retinoic acid or 48h with ILC2-conditioned or control media before GSIS.

In vivo glucose and insulin tolerance tests

For glucose tolerance tests (GTTs), mice were fasted for 6h in the morning and then injected with glucose (2 g per kg of body weight) intraperitoneally (i.p.). For insulin tolerance tests, mice were fasted for 3h in the morning and i.p. injected with human insulin (Novorapid, Novo Nordisk) (1U per kg of body weight) diluted in saline solution. Blood glucose was sampled from the mouse tail vein every 15–30 min following glucose or insulin injection and measured using a glucometer (Freestyle, Abbott Diabetes Care Inc.).

Glucose clamp studies

Glucose clamp studies were performed in freely moving mice as previously described (Wueest et al., 2014). Steady state glucose infusion rate was calculated once glucose infusion reached a constant rate with blood glucose concentrations of 5 mmol/l (80-90 min after the start of insulin infusion). Thereafter, blood glucose concentration was kept constant at 5 mmol/l for 15-20 min and glucose infusion rate was calculated. Glucose infusion rate and hepatic glucose production were calculated as previously described (Wueest et al., 2014). In order to assess tissue specific glucose uptake, a bolus (10 μCi) of 2-[1-14C] deoxyglucose was administered via catheter at the end of the steady state period. Blood was sampled 2, 15, 25, and 35 min after bolus delivery. Area under the curve of disappearing plasma 2-[1-14C] deoxyglucose was used together with tissue-concentration of phosphorylated 2-[1-14C] deoxyglucose to calculate glucose uptake.

In vivo IL-33 and anti-CD90.2 antibody treatments

Carrier-free recombinant murine IL-33 (Biolegend) was administered in 100 μL sterile saline by i.p. injection for one or three doses every other day at 500 ng per dose in chow diet mice. Mice fed a high fat diet received either saline or IL-33 for three doses every other day at 20 μg per kg of body weight. Metabolic tests were performed the day after the last injection. Mice were sacrificed one or two days after the last injection. For streptozotocin-induced diabetic C57BL/6 mice, only hyperglycemic mice (i.e., fasting blood glucose > 11 mM) were injected with IL-33 (starting from day 6 after streptozotocin injection). Anti-CD90.2 (30-H12; 250 μg)

antibody or corresponding IgG2b (RTK4530) (Biolegend) was administered in 125 μL sterile Phosphate Buffer Solution by i.p. injection twice every other day into BALB/c *Rag2*$^{-/-}$ mice or streptozotocin-induced diabetic C57BL/6 *Rag2*$^{-/-}$ mice (starting from day 6 after streptozotocin injection).

Flow cytometry

Clean handpicked islets were isolated and pooled together from at least 3 mice per condition. To obtain single cells, islets were gently dispersed with a 0.0125% trypsin-EDTA (GIBCO) solution for 2 min in a 37°C water bath, washed with cold FACS buffer (PBS with 0.5% BSA and 5 mM EDTA), centrifuged at 300 x g, 4°C for 5 min and resuspended in FACS buffer. After 15 min incubation with an Fc blocker (93; Thermo Fisher Scientific), single islet cells were stained with the appropriate antibodies or isotypes for 30 min at 4°C in the dark. The following antibodies were used: anti-CD45 (30-F11), anti-F4/80 (BM8), anti-CD11c (N418), anti-I-A/I-E (MHC-II) (M5/114.15.2), anti-CD3 (145-2C11), anti-B220 (RA3-6B2), anti-NKp46 (29A1.4), anti-Ly6G (1A8 – Ly6g), anti-CD90.2 (53-2.1), anti-KLRG1 (2F1), anti-CD103 (2E7) and anti-Sca-1 (D7) (from Thermo Fisher Scientific or Biolegend); anti-SIGLEC-F (E50-2440) (from BD bioscience) and anti-T1-ST2 (DJ8) (from mdbioproducts). ILC2 and ILC3 were identified based on the absence of PE-labeled lineage markers: anti-F4/80 (BM8), anti-CD11b (M1/70), anti-CD11c (N418), anti-Ly6G (RB6-8C5), anti-CD3 (145-2C11), anti-CD4 (GK1.5), anti-CD8a (53-6.7), anti-TCR beta (H57-597), anti-gamma delta TCR (eBioGL3), anti-CD19 (eBio1D3), anti-CD45R (RA3-6B2), anti-NKp46 (29A1.4), anti-NK1.1 (PK136) for C57BL/6 mice, anti-CD49b (DX5) for BALB/c mice and anti-Ter119 (Ter119) (all from Thermo Fisher Scientific). Anti-NKp46 was excluded from the lineage cocktail for the comparative study of ILC2/ILC3. DAPI^{+} cells and doublet were excluded from all analyses. For the detection of transcription factors, cells were fixed and stained using the Foxp3-staining kit (Thermo Fisher Scientific) according to the manufacturer's instructions and using anti-GATA3 (TWAJ) and anti-RORγ(t) (B2D) antibodies and a fixable viability dye (all from Thermo Fisher Scientific). For quantification of β and α cells in islets, cells were fixed and stained with anti-insulin (C27C9; Cell Signaling) and biotinylated anti-glucagon antibodies (Abcam). Multiparameter analyses were performed on a LSR-Fortessa flow cytometer (BD Bioscience) and analyzed with FlowJo software (Tree Star). For islet cell fraction sorting, anti-CD45 (30-F11) and anti-Sca-1 (D7) antibodies were used (from Thermo Fisher Scientific) to detect immune and mesenchymal cell populations, respectively. The β cell-enriched cell fraction was defined as cells showing a very high FSC-SSC profile (due to β cell insulin granularity). Cells were sort-purified with a FACS ARIA III cell sorter (BD Biosciences) using FACS Diva software (BD Biosciences).

Aldehyde dehydrogenase activity

Aldehyde dehydrogenase (ALDH) activity was determined using the ALDEFLUOR staining kit (StemCell Technologies) according to the manufacturer's instructions. Briefly, dispersed islet cells were divided into two tubes: one test and one control. In the control tube, ALDH inhibitor diethylaminobenzaldehyde (DEAB) was added and incubated for 15 min at 37°C. Then, fluorescent ALDH reagent was added in both tubes for 35 min at 37°C. Cells were washed twice and incubated with appropriate antibodies for FACS analysis.

Sort-purification of pancreatic ILC2

Whole pancreata of C57BL/6 mice were collected and pancreatic lymph nodes were removed under a stereomicroscope. Pancreata were cut into small pieces with razor blades and washed in fresh ice cold PBS. Pancreas pieces were incubated in 1.5 mL DMEM (GIBCO) containing 1 mg/ml Collagenase D (Roche) and 0.025 mg/mL DNAse I (Roche) at 37°C for 15 min. After incubation, pancreas pieces were washed with DMEM and supernatant was collected and passed through a 70 μm cell strainer (Corning). These steps were repeated 3 to 4 times. Isolated cells were washed with PBS and purified using a Percoll (GE Healthcare) gradient (40%/80%) at 20°C and 630 x g for 30 min. Cells of the interphase were collected and washed with PBS containing 3% FCS (Gibco Life Technologies). Pancreatic ILC2 identified as Lin-CD90.2^{+}Sca-1^{+}CD25^{+} cells were sorted with a FACS Aria (BD Biosciences) and re-analysis showed that cell purity was > 95%.

In vitro stimulation of pancreatic ILC2

For ILC2-conditioned media, approximately 2000 ILC2 were stimulated for 72h in RPMI containing 10% FBS with recombinant mouse IL-33 (10 ng/mL; Biolegend) and IL-2 (10 ng/mL; Thermo Fisher Scientific) in 96-well round bottom plates (Falcon) at 37°C and 10% CO_2. Supernatant was recovered and stored at -80°C for further experiments. For control medium, cell-free RPMI containing 10% FBS supplemented with the cytokines was incubated for 72h in the same conditions.

ILC2 transfer

Pancreatic ILC2 were purified from C57BL/6 mice that received *i.p.* three doses of IL-33 (500ng) every other day. 3 x 10^5 cells or PBS were immediately transferred to recipient *Rag2*$^{-/-}$*Il2rg*$^{-/-}$ mice by a single intravenous injection. 2h later and the next 2 days, recipient mice were treated with three doses of IL-33 (500ng) before performing GTTs and islet isolation for *ex vivo* GSIS assays.

Histological analyses

For β-Galactosidase detection, pancreata from *Il33*$^{Gt/+}$ and *Il33*$^{+/+}$ littermates were embedded in OCT Tissue Tek and frozen in liquid nitrogen. Pancreas sections were fixed and stained with chromogenic substrate X-Gal overnight using a LacZ Tissue staining kit (InvivoGen) according to the manufacturer's instructions. Sections were counterstained by nuclear Fast Red (Sigma), mounted with Mounting medium (Dako) and analyzed with a widefield microscope (Olympus BX63 Apollo). For β cell area analysis, pancreata (one section per animal) of saline- and IL-33-treated mice were fixed overnight in 4% paraformaldehyde at 4°C, followed by paraffin embedding. Sections were deparaffinized, re-hydrated and incubated overnight at 4°C with Guinea pig anti-insulin (Dako; A0564), followed by detection with Alexa657-conjugated Goat anti–guinea pig IgG (Thermo Fischer Scientific), counterstained with DAPI and mounted with Mounting medium (Dako). Pancreas sections were analyzed using a Hamamatsu flash 4.0 camera with a 4x Nikon Objective NA 0.2 and automatically scanned using a Nikon NiE with Prior PL-200 slide loading robot. Insulin^{+} area and distribution were calculated with NIS-Elements software (Nikon). For immunofluorescence staining of ILC2, pancreata of C57BL/6 *Rag2*$^{-/-}$ mice were embedded in OCT Tissue Tek and frozen in liquid nitrogen. Sections were fixed for 5 min in acetone at room temperature. They were then blocked with PBS containing 1% BSA (Sigma-Aldrich) for 30 min at room temperature and stained with Alexa657-conjugated anti-CD45.2 (104) and PE-conjugated anti-KLRG1 (2F1-KLRG1) from Biolegend and anti-NKp46 (R&D systems, AF2225) overnight at 4°C, followed by detection with Alexa488-conjugated Donkey anti-goat IgG (Thermo Fisher scientific) for 1h at room temperature and counterstained with DAPI. The slices were mounted (Fluoromount-G, Thermo Fisher Scientific) and analyzed with a widefield microscope (Leica DMI 4000).

Immunocytochemistry of islet cells

For staining of mouse islet cells, islet Sca-1^{+} cells and Sca-1^{-} cells were sort-purified; Sca-1^{-} cells were further separated between cells with a high FSC/SSC profile that are enriched in β cells and the rest. Following cytospin (Hettich) onto glass Polysine™ slides, cells were fixed with 4% paraformaldehyde (Sigma Aldrich) for 10 min, permeabilized with 0.1% Triton-X-100 for 5 min, blocked with PBS supplemented with 0.1% Tween 20, 1% BSA (Sigma Aldrich) and 0.3 M glycine for 30 min at room temperature. Cells were stained with Rabbit anti-Vimentin (Abcam; EPR3776) overnight at 4°C, followed by detection with Alexa488-conjugated Donkey anti-rabbit IgG (Biolegend) and counterstaining with DAPI, mounted with Mounting medium (Dako) and analyzed with a widefield microscope (Olympus BX63 Apollo).

Bone marrow-derived dendritic cells

4 x 10^6 bone marrow cells per well were cultured in a 6 well plate (Nunc) in supplemented IMDM (Sigma Aldrich) in the presence of 200 ng/ml FMS-like tyrosine kinase ligand (FLT3l, A. Rolink, University of Basel, Switzerland) at 37°C and 10% CO_2 as previously described (Brasel et al., 2000). After 6-7 days, BM-DCs were harvested, washed with PBS and used for overnight stimulation with IL-13 and Csf2 (10 ng/mL; Thermo Fisher Scientific) or IL-33 (10 ng/mL; Biolegend). Cells were harvested afterwards and used for RNA isolation.

Streptozotocin-induced β cell death

Streptozotocin (Sigma-Aldrich) was dissolved in citrate buffer (pH 4.5) and was injected once i.p. into 6 hour-fasted C57BL/6 mice (150 mg per kg of body weight) or C57BL/6 *Rag2*$^{-/-}$ mice (120 mg per kg of body weight).

In situ pancreatic perfusion

In situ pancreatic perfusion was performed in anesthetized mice treated with saline or IL-33 (three doses) as previously described (Maechler et al., 2002) with a perfusion rate of 1.5 ml/min (Maechler et al., 2002).

Protein measurement assays

Insulin concentrations were determined using a mouse/rat insulin kit (Mesoscale Discovery) according to the manufacturer's instructions. Mouse Csf2, IL-5 and human IL-33 concentrations were measured using the mouse GM-CSF Tissue Culture Kit, the V-plex mouse IL-5 and the U-plex human IL-33 (Mesoscale Discovery) according to the manufacturer's instructions. Mouse IL-33 was measured in 200 islets using the U-plex mouse IL-33 (Mesoscale Discovery); protocol was improved to achieve a lower limit of detection (LLOD) of 0.31 ± 0.07 pg/mL (Mean ± SD; n = 4). Mouse IL-13 was measured using mouse IL-13 Platinum ELISA (Thermo Fisher Scientific) according to the manufacturer's instructions.

RNA extraction and qRT-PCR

Total RNA was extracted using the Nucleo Spin RNA II Kit (Machery Nagel) or RNeasy Mini Kit (QIAGEN) for islets and bone marrow-derived dendritic cells, RNeasy Lipid Tissue (QIAGEN) for epididymal adipose tissue and PureLink RNA Micro Scale Kit (Invitogren) for sort-purified cells. cDNA was prepared with random hexamers (Microsynth) and Superscript II (Invitrogen) according to manufacturer's instructions. Gene expression was determined with TaqMan assays and the real time PCR system 7500 (Applied Biosystems). Data were normalized with the geometrical mean of 18S and β actin mRNA (18S was used for human samples) and quantified using the comparative 2-ΔΔCT method. The following TaqMan assays (ThermoFisher scientific) were used: *18s*: Mm99999901;

Actb: Mm00607939; *Acta2*: Mm00725412; *Aldh1a2*: Mm00501306; *Areg*: Mm00437583; *Ccl2*: Mm00441242; *Csf2*: Mm01290062; *Cxcl1*: Mm00433859; *Emr1*: Mm00802529; *Flt3*: Mm00439016; *Gcg*: Mm00801714; *Ifng*: Mm01168133; *Il10*: Mm01288386; *Il13*: Mm00434204; *Il1b*: Mm00434228; *Il1rl1*: Mm00516117; *Il4*: Mm00445258; *Il5*: Mm00439646; *Il22*: Mm01226722; *Il25*: Mm00499822; *IL33*: Hs01125943; *Il33*: Mm00505403; *Ins2*: Mm00731595; *Rara*: Mm01296312; *Rarb*: Mm01319677; *Rarg*: Mm00441091; *Rxra*: Mm00441185; *Tgfb*: Mm01178820; *Tslp*: Mm01157588; *Vim*: Mm01333430.

QUANTIFICATION AND STATISTICAL ANALYSIS

Data were routinely presented as mean ± standard error of mean (SEM). Significance was assessed by the methods specified in each individual figure legend using GraphPad Prism 7 (GraphPad Software). ''n'' numbers indicate biological replicates for *in vitro* experiments or number of mice for *in vivo* studies. Outliers were identified according to the two standard deviation method.